Biogeosciences Discuss., doi:10.5194/bg-2016-73, 2016
Manuscript under review for journal Biogeosciences
Published: 22 March 2016
© Author(s) 2016. CC-BY 3.0 License.

Biogeosciences Discussions
Open Access
EGU

An observational constraint on stomatal function in forests: evaluating coupled carbon and water vapor exchange with carbon isotopes in the Community Land Model (CLM 4.5)

Brett Raczka[1], Henrique F. Duarte[2], Charles D. Koven[3], Daniel Ricciuto[4], Peter E. Thornton[4], John C. Lin[2], David R. Bowling[1]

[1]{Dept. of Biology, University of Utah, Salt Lake City, Utah}

[2]{Dept. of Atmospheric Sciences, University of Utah, Salt Lake City, Utah}

[3]{Lawrence Berkeley National Laboratory, Berkeley, California}

[4]{Oak Ridge National Laboratory, Oak Ridge, Tennessee}

Correspondence to: B. Raczka (brett.raczka@utah.edu)

Abstract

Land surface models are useful tools to quantify contemporary and future climate impact on terrestrial carbon cycle processes, provided they can be appropriately constrained and tested with observations. Stable carbon isotopes of CO_2 offer the potential to improve model representation of the coupled carbon and water cycles because they are strongly influenced by stomatal function. Recently, a representation of stable carbon isotope discrimination was incorporated into the Community Land Model component of the Community Earth System Model. Here, we tested the model's capability to simulate whole-forest isotope discrimination in a subalpine conifer forest at Niwot Ridge, Colorado, USA. We distinguished between isotopic behavior in response to a decrease of $\delta^{13}C$ within atmospheric CO_2 (Suess effect) vs. photosynthetic discrimination (Δ_{canopy}), by creating a site-customized atmospheric CO_2 and $\delta^{13}C$ of CO_2 time series. We implemented a seasonally-varying V_{cmax} model calibration that best matched site observations of net CO_2 carbon exchange, latent heat exchange and biomass. The model accurately simulated observed $\delta^{13}C$ of needle and stem tissue, but underestimated the $\delta^{13}C$ of bulk soil carbon by 1-2 ‰. The model overestimated the multi-year (2006-2012) average Δ_{canopy} relative to prior data-based estimates by 5-6 ‰. The amplitude of the average seasonal cycle of Δ_{canopy} (i.e. higher in spring/fall as compared to summer) was correctly modeled but only with an alternative nitrogen limitation formulation for the model. The model

Biogeosciences Discuss., doi:10.5194/bg-2016-73, 2016
Manuscript under review for journal Biogeosciences
Published: 22 March 2016
© Author(s) 2016. CC-BY 3.0 License.

attributed most of the seasonal variation in discrimination to the net assimilation rate (A_n), whereas inter-annual variation in simulated Δ_{canopy} during the summer months was driven by stomatal response to vapor pressure deficit. Soil moisture did not influence modeled Δ_{canopy}. The model simulated a 10% increase in both photosynthetic discrimination and water use efficiency (WUE) since 1850 as a result of CO_2 fertilization, forced by constant climate conditions. This increasing trend in discrimination is counter to well-established relationships between discrimination and WUE. The isotope observations used here to constrain CLM suggest 1) the model overestimated stomatal conductance and 2) the default CLM approach to representing nitrogen limitation (post-photosynthetic limitation) was not capable of reproducing observed trends in discrimination. These findings demonstrate that isotope observations can provide important information related to stomatal function driven by environmental stress from VPD and nitrogen limitation.

1 Introduction

The net uptake of carbon by the terrestrial biosphere currently mitigates the rate of atmospheric CO_2 rise and thus the rate of climate change. Approximately 25% of anthropogenic CO_2 emissions are absorbed by the global land surface (Le Quéré et al., 2015), but it is unclear how projected changes in temperature and precipitation will influence the future of this land carbon sink (Arora et al., 2013; Friedlingstein et al., 2006). A major source of uncertainty in climate model projections results from the disagreement in projected strength of the land carbon sink (Arora et al., 2013). Thus, it is critical to reduce this uncertainty to improve climate predictions, and to better inform mitigation strategies (Yohe et al., 2007).

An effective approach to reduce uncertainties in terrestrial carbon models is to constrain a broad range of processes using distinct and complementary observations. Traditionally, terrestrial carbon models have relied primarily upon observations of land-surface fluxes of carbon, water and energy derived from eddy-covariance flux towers to calibrate model parameters and evaluate model skill. Flux measurements best constrain processes that occur at diurnal and seasonal time scales (Braswell et al., 2005; Ricciuto et al., 2008). Traditional ecological metrics of carbon pools (e.g. leaf area index, biomass) are also commonly used to provide independent and complementary constraints upon ecosystem processes at longer time scales (Ricciuto et al., 2011; Richardson et al., 2010). However, neither flux nor carbon pool

Biogeosciences Discuss., doi:10.5194/bg-2016-73, 2016
Manuscript under review for journal Biogeosciences
Published: 22 March 2016
© Author(s) 2016. CC-BY 3.0 License.

observations provide suitable constraints for the model formulation of plant stomatal function and the related link between the carbon and water cycles.

Stable carbon isotopes of CO_2 are influenced by stomatal activity in C3 plants (e.g. evergreen trees, deciduous trees), and thus provide a valuable but under-utilized constraint on terrestrial carbon models. Plants assimilate more of the lighter of the two major isotopes of atmospheric carbon (^{12}C vs. ^{13}C). This preference, termed photosynthetic discrimination (Δ_{canopy}), is primarily a function of two processes, CO_2 diffusion rate through the leaf boundary layer and into the stomata, and the carboxylation of CO_2. The magnitude of Δ_{canopy} is controlled by CO_2 supply (atmospheric CO_2 concentration, stomatal conductance) and demand (photosynthetic rate; Flanagan et al., 2012). In general, environmental conditions favorable to plant productivity result in higher Δ_{canopy} during carbon assimilation compared to unfavorable conditions. Plants respond to unfavorable conditions by closing their stomata and reducing the stomatal conductance which reduces $\Delta_{canopy.}$ Most relevant here, Δ_{canopy} responds to atmospheric moisture deficit (Andrews et al., 2012; Wingate et al., 2010), soil water content (McDowell et al., 2010), precipitation (Roden and Ehleringer, 2007) and nutrient availability. After carbon is assimilated, additional post-photosynthetic isotopic changes occur (Bowling et al., 2008; Brüggemann et al., 2011), but these impose a small influence on land-atmosphere isotopic exchange relative to photosynthetic discrimination.

The Niwot Ridge Ameriflux site, located in a sub-alpine conifer forest in the Rocky Mountains of Colorado, U.S.A., has a long legacy of yielding valuable datasets to test carbon and water functionality of land surface models using stable isotopes. Niwot Ridge has a 17-year record of eddy covariance fluxes of carbon, water, and energy, as well as environmental data (Hu et al., 2010; Monson et al., 2002) and a 10-year record of $\delta^{13}C$ of CO_2 in forest air (Schaeffer et al., 2008). From a carbon balance perspective, Niwot Ridge is representative of subalpine forests in Western North America that, in general, act as a carbon sink to the atmosphere (Desai et al., 2011). Western forests, make up a significant portion of the carbon sink in the United States (Schimel et al., 2002), yet this carbon sink is projected to weaken with projected changes in temperature and precipitation (Boisvenue and Running, 2010).

The Community Land Model (CLM), the land sub-component of the Community Earth System Model (CESM) has a comprehensive representation of biogeochemical cycling (Oleson et al., 2013) that can be applied across a range of temporal (hours to centuries) and spatial scales (site to global). A mechanistic representation of photosynthetic discrimination based

Biogeosciences Discuss., doi:10.5194/bg-2016-73, 2016
Manuscript under review for journal Biogeosciences
Published: 22 March 2016
© Author(s) 2016. CC-BY 3.0 License.

upon diffusion and enzymatic fractionation (Farquhar et al., 1989) was included in the latest release of CLM 4.5 (Oleson et al., 2013). An early version of CLM simulated carbon (but not carbon isotope) dynamics at Niwot Ridge with reasonable skill (Thornton et al., 2002). To date, we are not aware of any CLM-based studies that have used CO_2 isotopes at natural abundance to quantify the accuracy of the photosynthetic discrimination sub-model, or to evaluate the utility of CO_2 isotopes to constrain carbon and water cycle coupling.

Here, we evaluate the performance of the $^{13}C/^{12}C$ isotope discrimination sub-model within CLM 4.5 against a range of isotopic observations at Niwot Ridge, to examine what new insights an isotope-enabled model can bring upon ecosystem function. Specifically, we test whether CLM simulates the expected isotopic response to environmental drivers of CO_2 fertilization, soil moisture and atmospheric vapor pressure deficit (VPD). A previous analysis at Niwot Ridge showed a seasonal correlation between vapor pressure deficit (VPD) and photosynthetic discrimination (Bowling et al., 2014) which may suggest that leaf stomata are responding to changes in VPD, and influencing discrimination. We use CLM to test whether VPD is the primary environmental driver of isotopic discrimination, as compared to soil moisture and net assimilation rate. Next we determine whether including site-specific $\delta^{13}C$ of atmospheric CO_2 within the model simulation combined with simulated long term (multi-decadal to century) photosynthetic discrimination and simulated carbon pool turnover, accurately reproduces the measured $\delta^{13}C$ in leaf tissue, roots and soil carbon. We then use CLM to determine if the increase in atmospheric CO_2 since 1850 has led to an increase in WUE, and whether net assimilation or stomatal conductance is the primary driver of such a change. Finally, we ask what distinct insights site level isotope observations bring in terms of both model parameterization (i.e. stomatal conductance) and model structure as compared to the traditional observations (e.g. carbon fluxes, biomass).

2 Methods

We focus the description of CLM 4.5 (Section 2.1) upon photosynthesis, and its linkage to nitrogen, soil moisture and stomatal conductance (Section 2.1.1). Next we describe the model representation of carbon isotope discrimination by photosynthesis (Section 2.1.2). Because preliminary simulations demonstrated that model results were strongly influenced by nitrogen limitation, we used three separate nitrogen formulations (described in Section 2.1.2) to better diagnose model performance. Next, to provide context for subsequent descriptions of

Biogeosciences Discuss., doi:10.5194/bg-2016-73, 2016
Manuscript under review for journal Biogeosciences
Published: 22 March 2016
© Author(s) 2016. CC-BY 3.0 License.

site-specific model adjustments we describe the field site, Niwot Ridge, including the site level observations (Section 2.2) used to constrain model behavior and test model skill.

Patterns in plant growth and $\delta^{13}C$ of biomass are strongly influenced by atmospheric CO_2 and $\delta^{13}C$ of atmospheric CO_2 (δ_{atm}). Therefore we designed a site-specific synthetic atmospheric CO_2 product (Section 2.3.1) and δ_{atm} product (Section 2.3.2) for these simulations. The model setup and initialization procedure, intended to bring the system into steady state, is described in Section (2.3.3). This is followed by an explanation of the model calibration procedure that provided a realistic simulation of carbon and water fluxes (Section 2.4).

2.1 Community Land Model, Version 4.5

We used the Community Land Model, CLM 4.5 (Oleson et al., 2013), which is the land component of the Community Earth System Model (CESM) version 1.2 (https://www2.cesm.ucar.edu/models/current). Details regarding the Community Land Model can be found in (Mao et al., 2016; Oleson et al., 2013). Here, we emphasize the mechanistic formulation that controls photosynthetic discrimination (Δ_{canopy}) and factors that influence Δ_{canopy} including photosynthesis, stomatal conductance, water stress and nitrogen limitation. A list of symbols is provided in Table (1).

2.1.1 Net Photosynthetic Assimilation

The net carbon assimilation of photosynthesis, A_n is based on Farquhar et al., (1980) as,

$$A_n = \min(A_c, A_j, A_p) - Resp_d, \quad (1)$$

where A_c, A_j and A_p are the enzyme (Rubisco)-limited, light-limited, and product-limited rates of carboxylation respectively, and $Resp_d$ the leaf-level dark respiration. The enzyme limited rate is defined as

$$A_c = \frac{V_{cmax}(c_i - \Gamma_*)}{c_i + K_c(1+\frac{o_i}{K_o})}, \quad (2)$$

where c_i is the internal leaf partial pressure of CO_2, o_i = 0.209 P_{atm}, where P_{atm} is atmospheric pressure, and K_c, K_o and Γ_* are constants. The maximum rate of carboxylation at 25°C, V_{cmax25}, is defined as

$$V_{cmax25} = N_a \; F_{LNR} \; F_{NR} \; a_{R25}, \quad (3)$$

Biogeosciences Discuss., doi:10.5194/bg-2016-73, 2016
Manuscript under review for journal Biogeosciences
Published: 22 March 2016
© Author(s) 2016. CC-BY 3.0 License.

where N_a is the nitrogen concentration per leaf area, F_{LNR} the fraction of leaf nitrogen within the Rubisco enzyme, F_{NR} the ratio of total Rubisco molecular mass to nitrogen mass within Rubisco, and a_{R25} is the specific activity of Rubisco at 25°C. The V_{cmax25} is adjusted for leaf temperature to provide V_{cmax} in Eq. 2, used in the final photosynthetic calculation.

The carbon and water balance are linked through c_i by the stomatal conductance, g_s, following the Ball-Berry model as defined by Collatz et al., (1991),

$$g_s = m\frac{A_n}{c_s/P_{atm}}h_s + b\beta_t, \quad (4)$$

where m is the stomatal slope, c_s the partial pressure of CO_2 at the leaf surface and b the minimum stomatal conductance when the leaf stomata are closed. The variable $h_s = e_l/e_s$ is the leaf surface specific humidity with e_l the vapor pressure at the leaf surface and e_s the saturation vapor pressure inside the leaf. The variable β_t represents the level of soil moisture availability, which influences stomatal conductance directly, but also indirectly through A_n by multiplying V_{cmax} by β_t (Sellers et al., 1996). CLM calculates β_t as a factor (0-1, high to low stress) by combining soil moisture, the rooting depth profile, and a plant-dependent response to soil water stress as

$$\beta_t = \sum_i w_i r_i, \quad (5)$$

where w_i is a plant wilting factor for soil layer i and r_i is the fraction of roots in layer i. The plant wilting factor is scaled according to soil moisture and water potential, depending on plant functional type (PFT). Soil moisture is predicted based upon prescribed precipitation and vertical soil moisture dynamics (Zeng and Decker, 2009). The root fraction in each soil layer depends upon a vertical exponential profile controlled by PFT dependent root distribution parameters adopted from Zeng (2001).

The version of CLM used here has a 2-layer (shaded, sunlit) representation of the tree canopy. Photosynthesis and stomatal conductance are calculated separately for the shaded and sunlit portion and the total canopy photosynthesis is the potential gross primary productivity (GPP), CF_{GPPpot}. The total carbon available for new growth allocation (CF_{avail_alloc}) is defined as

$$CF_{avail\_alloc} = CF_{GPPpot} - CF_{GPP,mr} - CF_{GPP,xs}, \quad (6)$$

where $CF_{GPP,mr}$ is the carbon costs for maintenance respiration and $CF_{GPP,xs}$ is the carbon allocated to a pool responsible for meeting maintenance respiration demand during periods with

Biogeosciences Discuss., doi:10.5194/bg-2016-73, 2016
Manuscript under review for journal Biogeosciences
Published: 22 March 2016
© Author(s) 2016. CC-BY 3.0 License.

low or zero photosynthesis. In contrast, CF_{alloc}, is the actual carbon allocated to growth calculated from the available nitrogen and fixed C:N ratios for new growth (e.g. stem, roots, leaves). The downregulation of photosynthesis from nitrogen limitation, $f_{dreg,}$ is given by

$$f_{dreg} = \frac{CF_{avail\_alloc} - CF_{alloc}}{CF_{GPPpot}}. \quad (7)$$

2.1.2 Photosynthetic Carbon Isotope Discrimination

The canopy-level fractionation factor α_{psn} is defined as the ratio of $^{13}C/^{12}C$ within atmospheric CO_2 (R_a) and the products of photosynthesis (R_{GPP}) as $\alpha_{psn} = \frac{R_a}{R_{GPP}}$. The preference of C3 vegetation to assimilate the lighter CO_2 molecule during photosynthesis is simulated in CLM with two steps: diffusion of CO_2 across the leaf boundary layer and into the stomata, followed by enzymatic fixation to give the leaf-level fractionation factor:

$$\alpha_{psn} = 1 + \frac{4.4+22.6\frac{c_i^*}{c_a}}{1000}. \quad (8)$$

where c_i^* and c_a are the intracellular and atmospheric CO_2 partial pressure respectively. The variable c_i^* is marked with an asterisk to indicate the inclusion of nitrogen downregulation as defined as,

$$c_i^* = c_a - A_n\,(1 - f_{dreg})\,P_{atm}\,\frac{(1.4g_s)+(1.6g_b)}{g_b g_s} \quad (9)$$

where g_b is the leaf boundary layer conductance. The inclusion of the nitrogen downregulation factor f_{dreg} in the above expression reflects the two-stage process in which the potential photosynthesis and the actual photosynthesis are calculated within CLM and prevents a mismatch between the actual photosynthesis and the intracellular CO_2.

The sensitivity of preliminary model results to nitrogen limitation led us to test three distinct discrimination formulations (Table 2). The *limited nitrogen* formulation, was based on the default version of CLM 4.5 and included both nitrogen limitation and the nitrogen downregulation factor within the calculation of c_i^* as given in equation (9). In the second, *unlimited nitrogen* formulation, we allowed vegetation to have unlimited access to nitrogen ($CF_{GPPpot} = CF_{GPP}, f_{dreg} = 0$). Finally, in the *no downregulation discrimination* formulation, we included nitrogen limitation, but removed the downregulation factor f_{dreg} from equation (9).

Biogeosciences Discuss., doi:10.5194/bg-2016-73, 2016
Manuscript under review for journal Biogeosciences
Published: 22 March 2016
© Author(s) 2016. CC-BY 3.0 License.

In the *unlimited nitrogen* formulation, we use a different modifier on V_{cmax25} (described in section 2.4 and Fig. S1, S2) in the calibrated runs to give similar carbon flux, water flux and biomass as in the other two formulations, such that all three formulations have fluxes and biomass that are similar to what is observed at the site, and which presumably reflect nitrogen limitation. Thus the distinction between these three formulations can be viewed entirely of when nitrogen limitation is imposed in relation to photosynthesis: (1) *after photosynthesis* via a downregulation between potential and actual GPP (equation 7) that feeds back on the c_i/c_a used for isotopic discrimination but not on the stomatal conductance in the *limited nitrogen* formulation; (2) *before photosynthesis* via $V_{cmax,}$ which limits photosynthetic capacity affecting both c_i/c_a and stomatal conductance in the *unlimited nitrogen* formulation; and (3) *after photosynthesis with no effect on either* the c_i/c_a for isotopic discrimination or the stomatal conductance in the *no downregulation discrimination* formulation.

Carbon isotope ratios are expressed by standard delta notation,

$$\delta^{13}C_x = \left(\frac{R_x}{R_{VPDB}} - 1\right) \times 1000, \quad (10)$$

where R_x is the isotopic ratio of the sample of interest, and R_{VPDB} is the isotopic ratio of the Vienna Pee Dee Belemnite standard. The delta notation is dimensionless but expressed in parts per thousand (‰) where a positive (negative) value refers to a sample that is enriched (depleted) in $^{13}C/^{12}C$ relative to the standard. Because this is the only carbon isotope ratio we are concerned with in this paper, the '13' superscript is omitted for brevity in subsequent definitions using the delta notation. The canopy-integrated photosynthetic discrimination, $\Delta_{canopy,}$ is defined as the difference between the $\delta^{13}C$ of the atmospheric and assimilated carbon,

$$\Delta_{canopy} = \delta_{atm} - .\delta_{GPP.} \quad (11)$$

The difference between $\delta^{13}C$ of the total ecosystem respiration (ER) and GPP fluxes, called the isotope disequilibrium (Bowling et al., 2014), is defined as,

$$disequilibrium = \delta_{ER} - \delta_{GPP.} \quad (12)$$

The ecosystem-level water use efficiency (WUE) is defined as carbon assimilated (GPP) per unit water transpired (E_T) per unit land surface area,

$$WUE = \frac{GPP}{E_T}. \quad (13)$$

The intrinsic water use efficiency ($iWUE$) from leaf-level physiological ecology is defined as,

Biogeosciences Discuss., doi:10.5194/bg-2016-73, 2016
Manuscript under review for journal Biogeosciences
Published: 22 March 2016
© Author(s) 2016. CC-BY 3.0 License.

$$iWUE = \frac{A}{g_s}\ , \tag{14}$$

where A is the carbon assimilated per unit leaf area and g_s is the stomatal conductance. CLM calculates g_s (Equation 4) for shaded and sunlit portions of the canopy separately, therefore an overall conductance was calculated by weighting the conductance by sunlit and shaded leaf areas and is used in this manuscript.

2.2 Niwot Ridge and site-level observations

Site-level observations and modeling were focused on the Niwot Ridge Ameriflux tower, a sub-alpine conifer forest located in the Rocky Mountains of Colorado, U.S.A. The forest is approximately 110 years old and consists of lodgepole pine, Engelmann spruce, and subalpine fir. The site is located at an elevation of 3050 m above sea level, with mean annual temperature of 1.5°C and precipitation of 800 mm, in which approximately 60% is snow. More site details are available elsewhere (Hu et al., 2010; Monson et al., 2002). Flux and meteorological data were obtained from the Ameriflux archive (http://ameriflux.lbl.gov/).

Net carbon exchange (NEE) observations from the flux towers were partitioned into component fluxes of GPP and ER according to methods described by Reichstein et al., (2005) and Lasslop et al., (2010) using an online tool provided by the Max Planck Institute (http://www.bgc-jena.mpg.de/~MDIwork/eddyproc/). Seasonal patterns in δ_{GPP} and δ_{ER} were derived from measurements as described by (Bowling et al., 2014). Observations of $\delta^{13}C$ of biomass (Schaeffer et al., 2008) and carbon stocks (Bradford et al., 2008; Scott-Denton et al., 2003) were compared to model simulations. Schaeffer et al., (2008) reported soil, leaf and root observations specific to each conifer species, however, the observed mean and standard error for all species were used for comparison because CLM treated all conifer species as a single PFT.

2.3 Atmospheric CO_2, isotope forcing and initial vegetation state

2.3.1 Site-specific atmospheric CO_2 concentration time series

Global average atmospheric CO_2 concentrations increased roughly 40% from 1850 to 2013 (from 280 to 395 ppm). The standard version of CLM 4.5 includes an annually and globally averaged time series of this CO_2 increase, however, this does not capture the observed seasonal variation of ~10 ppm at Niwot Ridge (Trolier et al., 1996). Therefore we created a

Biogeosciences Discuss., doi:10.5194/bg-2016-73, 2016
Manuscript under review for journal Biogeosciences
Published: 22 March 2016
© Author(s) 2016. CC-BY 3.0 License.

site-specific atmospheric CO_2 time series (Figure 1) to provide a seasonally realistic atmosphere at Niwot Ridge. Observations were used to create the synthetic product from 1968-2013 by binning flask observations into 20 evenly spaced points each year. These flask observations were taken weekly from Niwot Ridge (Dlugokencky et al., 2015). Prior to 1968, a polynomial fit of the annualized CLM product was created and then adjusted by 1.5 ppm to account for the average difference between the CLM product and the Niwot Ridge observations during those years. Next, the average multi-year seasonal cycle based on the de-trended flask data after 1968 was added to every year of this annualized polynomial before 1968. Finally, the synthetic atmospheric CO_2 time series (pre 1968) was populated with 20 evenly spaced points in time each year.

2.3.2 Customized $\delta^{13}C$ atmospheric CO_2 time series

As atmospheric CO_2 has increased, the $\delta^{13}C$ of atmospheric CO_2 (δ_{atm}) has become more depleted (Francey et al., 1999), and this change has occurred at Niwot Ridge at -0.25 ‰ per decade (Bowling et al., 2014). The δ_{atm} also varies seasonally, and depends on latitude (Trolier et al., 1996). However, CLM 4.5 as released assigned a constant $\delta^{13}C$ of -6 ‰. We therefore created a synthetic time series of δ_{atm} from 1850-2013 (Figure 1). From 1990-2013 this was based upon the flask observations (White et al., 2015) as described in Section 2.3.1. A similar approach to the atmospheric CO_2 synthetic time series (Section 2.3.1) was applied here to create the synthetic δ_{atm}. After 1990 the flask data were binned into 20 evenly spaced points each year. Prior to 1990 the inter-annual variation was based upon a polynomial fit to ice core data from Law Dome (Francey et al., 1999; see also Rubino et al., 2013). The polynomial was adjusted by 0.20 ‰ to account for the inter-hemispheric difference identified during the common years (1990-1996) between the ice core and flask data. Next the average seasonal cycle (1990-2013) of δ_{atm} was added to the adjusted polynomial prior to 1990. The synthetic time series was populated from 1850-1989 with 20 evenly spaced points each year based upon the adjusted polynomial with seasonal cycle included. As released, CLM 4.5 was not compatible with time varying δ_{atm}, therefore we modified the source code by following the model procedure for reading in time-varying ^{14}C. The modified code was designed to temporally interpolate the δ_{atm} time series for each time step of the model. This interpolated

Biogeosciences Discuss., doi:10.5194/bg-2016-73, 2016
Manuscript under review for journal Biogeosciences
Published: 22 March 2016
© Author(s) 2016. CC-BY 3.0 License.

value was then passed into the photosynthetic discrimination calculation to represent the time-varying δ_{atm}.

2.3.3 Model Initialization

We performed an initialization to transition the model from near bare-ground conditions to present day carbon stocks and LAI that allowed for proper evaluation of isotopic performance. This was implemented in 4 stages: 1) accelerated decomposition (1000 model years) 2) normal decomposition (1000 model years) 3) parameter calibration (1000 model years) and 4) transient simulation period (1850-2013). The first two stages were pre-set options within CLM with the first stage used to accelerate the equilibration of the soil carbon pools, which require a long period to reach steady state (Thornton and Rosenbloom, 2005). The parameter calibration stage was not a pre-set option but designed specifically for our analysis. For this we introduced a seasonally varying V_{cmax} that scaled the simulated GPP and ecosystem respiration fluxes to present day observations (Section 2.4). In the transient phase, we introduced time-varying atmospheric conditions from 1850-2013 including nitrogen deposition (CLM provided), atmospheric CO_2, and δ_{atm} (site-specific as described above). Environmental conditions of temperature, precipitation, relative humidity, radiation, and wind speed were taken from the Niwot Ridge flux tower observations from 1998-2013 and then cycled continuously for the entirety of the initialization process. We used a scripting framework (PTCLM) that automated much of the workflow required to implement several of these stages in a site level simulation (Mao et al., 2016; Oleson et al., 2013).

2.4 Specific model details and model calibration

We used PTCLM (e.g. Mao et al., 2016) to create site specific weather conditions and initial conditions for CLM 4.5. This version of CLM included a fully prognostic representation of carbon and nitrogen within its vegetation, litter and soil biogeochemistry. We used the Century model representation for soil (3 litter and 3 soil organic matter pools) with 15 vertically resolved soil layers. Nitrification and prognostic fire were turned off. Our initial simulations used prognostic fire, but we found that simulated fire was overactive leading to low simulated biomass compared to observations. Although Niwot Ridge has been subject to disturbance from

Biogeosciences Discuss., doi:10.5194/bg-2016-73, 2016
Manuscript under review for journal Biogeosciences
Published: 22 March 2016
© Author(s) 2016. CC-BY 3.0 License.

fire and harvest in the past, ultimately our final simulations did not include either fire or harvest disturbance because the last disturbance occurred over 100 years ago (early 20th century logging; Monson et al., 2005).

Ecosystem parameter values (Table 3) used here were based upon the temperate evergreen needleleaf plant functional type (PFT) within CLM. These values were based upon observations reported by White et al., (2000) intended for a wide range of temperate evergreen forests, and by Thornton et al., (2002) for Niwot Ridge. For this analysis two site-specific parameter changes were made. First, the e-folding soil decomposition parameter was increased from 5 to 20 meters. This parameter is a length-scale for attenuation of decomposition rate for the resolved soil depth from 0 to 5 meters where an increased value effectively increases decomposition at depth, thus reducing total soil carbon and more closely matching observations. Second, we performed an empirical photosynthesis scaling (equation 15, below) that reduced the simulated photosynthetic flux, as guided by eddy covariance observations. Consequently, all downstream carbon pools and fluxes including ecosystem respiration, aboveground biomass, and leaf area index which provided a better match to present day observations. This approach also removed a systematic overestimation of winter photosynthesis. The model simulations without the photosynthetic scaling are referred to within the text and figures as the *uncalibrated* model, whereas model simulations that include the photosynthetic scaling are referred to as the *calibrated* model. The source code was modified for this scaling approach by reducing V_{cmax} at 25° Celsius,

$$V_{cmax25} = N_a \; F_{LNR} \; F_{NR} \; a_{R25} \; f_{df}, \tag{15}$$

where f_{df} is the photosynthetic scaling factor, and all other parameters are identical to equation (3). These parameters were constant for the entirety of the simulations except for f_{df}, an empirically derived time dependent parameter ranging from 0-1. The value was set to zero to force photosynthesis to zero between November 13th and March 23rd, consistent with flux tower observations where outside of this range GPP > 0 was never observed. During the growing season period (GPP>0) within days of year 83-316, f_{df} was calculated as

$$f_{df} = \frac{observed\ GPP(day\ of\ year)}{simulated\ GPP(day\ of\ year)}, \quad 82 < day\ of\ year < 317 \tag{16}$$

where the *observed GPP* was the daily average calculated from the partitioned flux tower observations (Reichstein et al., 2005) from 2006-2013, and the *simulated GPP* was the daily average of the unscaled value during the same time. A polynomial was fit to equation (16) that

Biogeosciences Discuss., doi:10.5194/bg-2016-73, 2016
Manuscript under review for journal Biogeosciences
Published: 22 March 2016
© Author(s) 2016. CC-BY 3.0 License.

represented f_{df} for 1) both the *limited nitrogen* and *no downregulation discrimination formulation* and 2) the *unlimited nitrogen* formulation (Figure S1). Note that CLM already includes a *daylength factor* that also adjusts the magnitude of V_{cmax} according to time of year, however, that default parameterization alone was not sufficient to match the observations.

3 Results & Discussion

This section is organized into four parts. First the calibrated model performance is evaluated against observed bulk carbon pool and bulk carbon flux behavior (Section 3.1.1), and against the observed $\delta^{13}C$ within carbon pools (Section 3.1.2). Second, the simulated photosynthetic discrimination is evaluated for multi-decadal trends (Section 3.2.1), magnitude (Section 3.2.2) and seasonal patterns (Section 3.2.3), including the environmental factors that were most responsible for driving the seasonal discrimination (Section 3.2.4). Third, we discuss how isotope observations can be used to guide model development related to nitrogen limitation (Section 3.3). Finally, we evaluate the capability of the model to reproduce the magnitude and trends of disequilibrium (Section 3.4).

3.1 Calibrated model performance

3.1.1 Fluxes & carbon pools

The CLM model was successful at simulating GPP, ER, and latent heat fluxes (Fig. 2), leaf area index (LAI), and aboveground biomass (Fig. 3), but only following site-specific calibration. The *uncalibrated* simulation (*limited nitrogen* formulation) overestimated LAI (39 %), aboveground biomass (48%), average peak warm season GPP (15%), and average peak warm season ER (40%) and overestimated cold-season GPP by 200 gC m^{-2} yr^{-1}. The *calibrated* simulation was much closer to the observations for LAI and aboveground biomass (Figure 3). The calibrated peak warm and cold season GPP, and warm season ER matched observations. The simulated latent heat fluxes were relatively insensitive to the calibration. Overall the simulated latent heat during the warm season overestimated the observations by 10% and underestimated by 10% during the cold season. Similar improvement was observed after calibration for the *unlimited nitrogen* run (not shown).

Biogeosciences Discuss., doi:10.5194/bg-2016-73, 2016
Manuscript under review for journal Biogeosciences
Published: 22 March 2016
© Author(s) 2016. CC-BY 3.0 License.

The calibration also eliminated erroneous winter GPP. In general, terrestrial carbon models tend to overestimate photosynthesis during cold periods for temperate/boreal conifer forests (Kolari et al., 2007), including Niwot Ridge (Thornton et al., 2002). One approach to correct for this is to include an acclimatization temperature (e.g. Flanagan et al., 2012) that reduces photosynthetic capacity during the spring and fall. The CLM 4.5 model includes functionality to adjust the photosynthetic capacity, including both a temperature acclimatization and a day length factor that reduces V_{cmax} (Bauerle et al., 2012; Oleson et al., 2013). However, this alone was not sufficient to match the observed fluxes. Although our calibration approach forced V_{cmax} to zero during the winter, it did not solve the underlying mechanistic shortcoming. A more fundamental approach should address either cold inhibition (Zarter et al., 2006) of photosynthesis or root access to soil moisture (Monson et al., 2005) to achieve the photosynthetic reduction. Nevertheless, within the confines of our study area, our calibration approach was sufficient to provide a skillful representation of photosynthesis and provided a sufficient testbed for evaluating carbon isotope behavior.

3.1.2 $\delta^{13}C$ of carbon pools

The model performed better simulating $\delta^{13}C$ biomass of bulk needle tissue, roots and soil carbon (Figure 4) for the *unlimited nitrogen* and no *downregulation discrimination* cases as compared to the *limited nitrogen* case. When nitrogen limitation was included the model underestimated $\delta^{13}C$ of sunlit needle tissue (1.8 ‰), bulk roots (1.0 ‰), and organic soil carbon (0.7‰). All simulations fell within the observed range of $\delta^{13}C$ in needles that span from -28.7 ‰ (shaded) to -26.7 (sunlit). This vertical pattern in $\delta^{13}C$ of leaves is common (Martinelli et al., 1998) and results from vertical differences in nitrogen allocation and photosynthetic capacity. The model results integrated the entire canopy and ideally should be closer to sun leaves (as in Figure 4) given that the majority of photosynthesis occurs near the top of the canopy.

Model simulations of $\delta^{13}C$ of living roots were ~1 ‰ more negative as compared to the structural roots. This range in $\delta^{13}C$ results from decreasing δ_{atm} with time (Suess effect, Figure 1). The living roots had a relatively fast turnover time of carbon within the model, whereas the structural roots had a slower turnover time and reflected an older (more enriched δ_{atm}) atmosphere. The *limited nitrogen* simulation was a poor match to observations relative to the others (Figure 4, middle panel).

Biogeosciences Discuss., doi:10.5194/bg-2016-73, 2016
Manuscript under review for journal Biogeosciences
Published: 22 March 2016
© Author(s) 2016. CC-BY 3.0 License.

There was an observed vertical gradient in $\delta^{13}C$ of soil carbon (-24.9 to -26 ‰) with more enriched values at greater depth (Figure 4, right panel). This vertical gradient is commonly observed (Ehleringer et al., 2000). Simulated $\delta^{13}C$ of soil carbon was most consistent with the organic horizon observations. There are a wide variety of post-photosynthetic fractionation processes in the soil system (Bowling et al., 2008; Brüggemann et al., 2011) that are not considered in the CLM 4.5 model, so the match with observations is perhaps fortuitous.

3.2 Photosynthetic discrimination

3.2.1 Decadal changes in photosynthetic discrimination and driving factors

All modeled carbon pools showed steady depletion in $\delta^{13}C$ since 1850 (coinciding with the start of the transient phase of simulations, Figure 4). For the *limited nitrogen* run, there was a decrease in $\delta^{13}C$ of 2.3 ‰ for needles, 2.3 ‰ for living roots, and 0.1 ‰ for soil carbon. This occurred because of 1) decreased δ_{atm} (Suess effect, Figure 1) and 2) increased photosynthetic discrimination. We quantified the contribution of the Suess effect by performing a control run with constant δ_{atm}, and kept other factors the same (Figure 5). Approximately 70% of the reduction in $\delta^{13}C$ of needles occured due to the Suess effect, and the remaining 30% was caused by increased photosynthetic discrimination. This occurred as plants responded to CO_2 fertilization as illustrated in Figure (6). The model indicated that plants responded to increased atmospheric CO_2 (~40% increase) by decreasing stomatal conductance (Equation 4) by 20% for the *limited nitrogen* run and 30% for the *unlimited nitrogen* run (Figure 6B) with associated change in c_i/c_a (Figure 6A). Other influences upon stomatal conductance were less significant, including A_n (+ 10% *limited nitrogen*, -10% *unlimited nitrogen*, Figure 6D), soil moisture availability (2-3%, Figure 6E), and negligible changes in relative humidity (potential climate change effects are neglected due to methodological cycling of weather data). This finding that stomatal conductance responded to atmospheric CO_2 is consistent with both tree ring studies (Saurer et al., 2014) and flux tower measurements (Keenan et al., 2013).

The effect of CO_2 fertilization, and associated response of stomatal conductance and net assimilation led to a multi-decadal increase in c_i/c_a for all model formulations (Figure 6A). The c_i/c_a increased from 0.71 to 0.76, 0.67 to 0.71 and 0.66 to 0.68 for the *limited nitrogen*, *unlimited nitrogen* and *no downregulation discrimination* formulations respectively from 1850-2013. All simulations therefore suggested an *increase* in photosynthetic discrimination. This increase in discrimination falls in between two hypotheses posed by Saurer et al., (2004) regarding stomatal

Biogeosciences Discuss., doi:10.5194/bg-2016-73, 2016
Manuscript under review for journal Biogeosciences
Published: 22 March 2016
© Author(s) 2016. CC-BY 3.0 License.

response to increased CO_2: 1) reduction in stomatal conductance causes c_i to proportionally increase with c_a keeping c_i/c_a constant and 2) minimal stomatal conductance response where c_i increases at the same rate as c_a (constant $c_a - c_i$) causing c_i/c_a to increase. Our simulation generally agrees with the observed trend in c_i/c_a as estimated from tree ring isotope measurements from a network of European forests (Frank et al., 2015). When controlled for trends in climate, Frank et al. (2015) found that c_i/c_a was approximately constant during the last century. If the Niwot Ridge multi-decadal warming trends in temperature and humidity (Mitton and Ferrenberg, 2012) were included in the CLM simulations the stomatal response may have been stronger thereby holding c_i/c_a constant.

The simulated stomatal closure in response to CO_2 fertilization led to an increase in iWUE and WUE of approximately 10-15% (Figure 6F). This is consistent with model and observation-based studies (Ainsworth and Long, 2005; Franks et al., 2013; Peñuelas et al., 2011) which indicate a 15-20% increase in iWUE for forests. This suggested that the vegetation at Niwot Ridge has some ability to maintain net ecosystem productivity when confronted with low soil moisture, low humidity conditions. Ultimately, whether Niwot Ridge maintains the current magnitude of carbon sink (Figure 2) will depend upon the severity of drought conditions, as improvements in WUE, in general, are only likely to negate weak to moderate levels of drought (Frank et al., 2013).

The simultaneous increase in both simulated photosynthetic discrimination and iWUE conflicts with observations where increases in iWUE are typically linked with weakening discrimination (e.g. Saurer et al., 2004). However, under certain conditions iWUE and discrimination can vary independently because of variation in leaf evaporative demand (VPD) and atmospheric CO_2 (Seibt et al., 2008). In general, an increase in atmospheric CO_2 alone tends to increase iWUE because of reduced stomatal conductance, however, the impact upon discrimination is close to neutral because the increased supply of CO_2 external to the leaf is offset by reduced stomatal conductance (Saurer et al., 2004) The VPD likely plays an important role in determining the final trends for iWUE and discrimination, where an increasing VPD should further reduce stomatal conductance thereby promoting the well-established relationship (increasing iWUE, decreasing discrimination). In contrast, a weak or decreasing trend in VPD should promote the opposite relationship (increasing iWUE, increasing discrimination). For example, simultaneous increase in iWUE and discrimination were identified at Harvard Forest (Belmecheri et al., 2014). Here, we do not consider multi-decadal trends in climate, therefore

Biogeosciences Discuss., doi:10.5194/bg-2016-73, 2016
Manuscript under review for journal Biogeosciences
Published: 22 March 2016
© Author(s) 2016. CC-BY 3.0 License.

increasing atmospheric CO_2 must be the primary driver for the simulated simultaneous increase in discrimination and iWUE at Niwot Ridge (Figure 6). These trends in WUE and discrimination simulated at Niwot Ridge have also been found in a fully-coupled, isotope enabled, global CESM simulation (Figure S2). Specifically, a random sample of land model grid cells representing conifer species in British Columbia (lat: 52.3° N, lon: -122.5° W) and Quebec (lat: 49.5° N, lon: -70.0° W) all showed an increase in photosynthetic discrimination and a 10% increase in WUE from 1850-2005. These randomly chosen grid cells are likely better analogs to the site-level simulations described here because they represent boreal conifer forests, whereas the grid cells that are in the Niwot Ridge area were heterogeneous in land cover (e.g. tundra, grassland, forest) and a poor representation of conifer forest.

The trends in the global simulation suggest that the site level trends are not isolated to the specific conditions of Niwot Ridge, but are a function of the model formulation. There is a relationship between iWUE and c_i/c_a (discrimination) as derived from equation (9) within the CLM model,

$$\frac{c_i^*}{c_a} \cong 1 - \frac{1.6}{c_a}\, iWUE. \qquad (17)$$

The full derivation is provided in the supplement. Note that increasing iWUE is consistent with decreasing c_i/c_a ($\sim\alpha_{psn}$) and therefore consistent with established understanding between trends in iWUE and discrimination. However, this trend imposed by iWUE can be neutralized by increasing c_a. During the course of the Niwot Ridge simulation iWUE increased between 10-20% (Figure 6), however, c_a increased by 40% during that same time (1850-2013).

3.2.2 Magnitude of photosynthetic discrimination

The simulated photosynthetic discrimination (Fig. 7) was significantly larger than an estimate derived from observations and an isotopic mixing model (Bowling et al., 2014). For brevity we refer to the estimates based on the Bowling et al. (2014) method as 'observed' discrimination but highlight that they are derived from observations and not directly measured. On average, the simulated monthly growing season mean canopy discrimination was greater than observed values by 6.3, 6.1, and 5.1‰ for the *limited nitrogen*, *unlimited nitrogen*, and *no downregulation discrimination* formulations respectively. The model-observation mismatch in discrimination, despite model-observation agreement to biomass, carbon and latent heat flux

Biogeosciences Discuss., doi:10.5194/bg-2016-73, 2016
Manuscript under review for journal Biogeosciences
Published: 22 March 2016
© Author(s) 2016. CC-BY 3.0 License.

tower observations (Figure 2) highlights the independent, and useful constraint isotopic observations provide for evaluating model performance. Specifically, the overestimation of discrimination may suggest the stomatal slope in the Ball-Berry model (m=9 in Eq. 4) used for these simulations was too high. This is supported by Mao et al., (2016), who found a reduced stomatal slope (m=5.6) was necessary for CLM 4.0 to match observed $\delta^{13}C$ in an isotope labeling study of loblolly pine forest in Tennessee. The stomatal slope was also found to be important to match discrimination behavior in the ISOLSM model (Aranibar et al., 2006), a predecessor to CLM.

The mixing model approach estimate of Δ_{canopy} (17 ‰), combined with δ_{atm} (-8.25 ‰) implies a $\delta^{13}C$ of biomass between -26 to -25 ‰. This range of values is only slightly more enriched than the observed ranges of $\delta^{13}C$ of needle and root biomass (-27 to -26 ‰). The fact that the different approaches to measure discrimination differ by only 1 ‰, whereas CLM simulates a Δ_{canopy} that is 5-6 ‰ greater than the mixing model discrimination, strongly suggests that the model has overestimated discrimination from 2006-2012. Therefore what appeared to be a successful match between the simulated and observed $\delta^{13}C$ biomass, may in fact have been fortuitously reached through compensating during the simulation. A multi-decadal time series of discrimination estimates inferred from $\delta^{13}C$ of tree rings (Saurer et al., 2014; Frank et al., 2015) would be useful to investigate this mismatch as a function of time, but these data are not presently available.

It is likely that the overestimation of modeled discrimination originates from a lack of response of stomatal conductance to environmental conditions. This could be a result of one or several of the following within the model: 1) parameter calibration issue -the stomatal slope value is too high, 2) boundary condition issue -the multi-decadal trends in climate (e.g. VPD) have not been included in the simulation or 3) model structural issue -the Ball-Berry representation of stomatal conductance is not sensitive enough to changes in environmental conditions (e.g. VPD, soil moisture). It has been shown that VPD may be an improved predictor of g_s (Katul et al., 2000; Leuning, 1995) and discrimination (Ballantyne et al., 2010, 2011) as compared to relative humidity, currently used in CLM 4.5. It would be worthwhile to clearly identify in future work which of the three scenarios is responsible for overestimation of the discrimination.

Biogeosciences Discuss., doi:10.5194/bg-2016-73, 2016
Manuscript under review for journal Biogeosciences
Published: 22 March 2016
© Author(s) 2016. CC-BY 3.0 License.

3.2.3 Seasonal pattern of photosynthetic discrimination

The model formulations that did not explicitly consider the influence of nitrogen limitation upon discrimination (*unlimited nitrogen*, *no downregulation discrimination*) were most successful at reproducing the seasonality of discrimination (Figure 7; Figure S3). In general, the observed discrimination was stronger during the spring and fall and weaker during summer. This observed Δ_{canopy} seasonal range (excluding November) varied from 16.5 to 18 ‰ using Reichstein partitioning (Figure 7), and was more pronounced using Lasslop partitioning (16.5 to 23 ‰) (Figure S3). The nitrogen limited simulated Δ_{canopy} had no seasonal trend whereas the *unlimited nitrogen* and *no downregulation discrimination* simulations both ranged from 21 to 23 ‰.

The main driver of the seasonality of discrimination was the net assimilation (A_n) for the *unlimited nitrogen* formulation (Figure 8). This was evident given the inversely proportional relationship between the simulated fractionation factor (α_{psn}) and A_n, consistent with equation (9). Stomatal conductance (g_s) also influenced the seasonal pattern. The most direct evidence for this was during the period between days 175-200 (Figure 8), where A_n descended from its highest value (favoring higher α_{psn}), and g_s abruptly ascended to its highest value (favoring higher α_{psn}). The α_{psn} responded to this increase in g_s with an abrupt increase by approximately 0.003 (3 ‰). Similarly, the *limited nitrogen* simulation seasonal discrimination pattern was shaped by both A_n and g_s, although the magnitude for both was approximately 30% higher during the summer months as compared to the unlimited nitrogen simulation. This was because the calibrated V_{cmax} value for the *limited nitrogen* simulation was much higher than for the *unlimited nitrogen* simulation (section 3.3). The difference in α_{psn} between the two model formulations coincided with the sharp increase in f_{dreg} between days 125 and 275, providing strong evidence that the downregulation mechanism within the *limited nitrogen* formulation led to increased discrimination during the summer. Therefore, it follows that the nitrogen downregulation mechanism was the root cause of the small range in simulated seasonal cycle discrimination for the *limited nitrogen* formulation, which was inconsistent with the observations.

3.2.4 Environmental factors influencing seasonality of discrimination

The simulated Δ_{canopy} was driven primarily by net assimilation (A_n), followed by vapor pressure deficit (VPD) (Fig. 9). The correlation between VPD and Δ_{canopy} was strongest for

Biogeosciences Discuss., doi:10.5194/bg-2016-73, 2016
Manuscript under review for journal Biogeosciences
Published: 22 March 2016
© Author(s) 2016. CC-BY 3.0 License.

the *unlimited nitrogen* simulation, where the range in monthly average Δ_{canopy} spanned values from 22 to 18 ‰ (Figure 9, middle row). This resembled the observed range in response based upon a fitted relationship from Bowling et al., (2014) that spanned from roughly 16 to 19 ‰ (left panels of Fig. 9), although with a consistent discrimination bias. The correlation between VPD and $\Delta_{canopy,}$ however, does not demonstrate causality. If that were the case, given that g_s is a function of VPD (h_s term in Eq. 4) and discrimination is a function of g_s (Eq. 8), a similar relationship should have existed between g_s and $\Delta_{canopy.}$ This, in fact, was not the case. Overall, the influence of g_s (responding to VPD) (R-value = -0.50) was secondary to A_n (R-value = -0.77) in driving changes in discrimination (Figure 9). The model suggested that the range in seasonal discrimination (intra-annual variation) was driven by the magnitude of A_n based on the inverse relationship between A_n and $\Delta_{canopy,}$ (equation 9) illustrated by the separation between months of low photosynthesis (October, May) vs. high photosynthesis (June, July, August). During times of relatively low photosynthesis A_n also drove the inter-annual variation in Δ_{canopy}. On the other hand, g_s (VPD) was most influential in driving the inter-annual variation of discrimination during the summer months only, judging by the directly proportional relationship during the months of June, July and August. Strictly speaking, g_s is a function of h_s (leaf specific humidity) and not atmospheric VPD in CLM. However, the two are closely related and the relationship between either variable (atmospheric VPD or simulated leaf humidity) to Δ_{canopy} was similar (Figure S4).

The *limited nitrogen* formulation did not produce as wide a range in discrimination as compared to the observations (Figure 9, top row). Part of this result was attributed to the lack of response between A_n and $\Delta_{canopy.}$ In this case, the discrimination did not decrease with increasing A_n because the signal was muted by the countering effect of $f_{dreg.}$ The *limited nitrogen* formulation was, however, able to reproduce the same discrimination response to $g_{s.}$ as compared to the other model formulations. The tendency for the limited nitrogen model to simulate discrimination response to g_s and not to A_n may negatively impact its ability to simulate multi-decadal trends in discrimination. This may not be a major detriment to sites such as Niwot Ridge which have maintained a consistent level of carbon uptake during the last decade, and is likely more susceptible to environmental impact upon stomatal conductance. However, sites that have shown a significant increase in assimilation rate (e.g. Harvard Forest; (Keenan et al., 2013)) are less likely to be well represented by this model formulation.

Biogeosciences Discuss., doi:10.5194/bg-2016-73, 2016
Manuscript under review for journal Biogeosciences
Published: 22 March 2016
© Author(s) 2016. CC-BY 3.0 License.

Given the dependence of forest productivity at Niwot Ridge on snowmelt (Hu et al., 2010), it was surprising that the model simulated minimal soil moisture stress (Fig. 8e) and therefore minimal discrimination response to soil moisture. However, this finding was consistent with Bowling et al., (2014), who did not find an isotopic response to soil moisture. In addition, lack of response to change in soil moisture may not be indicative of poor performance of the isotopic sub-model performance, but rather an effect of the hydrology sub-model (Duarte et al. (in prep)). However, a comparison of observed soil moisture at various depths at Niwot Ridge generally agrees with the CLM simulated soil moisture (not shown), suggesting the lack of model response to soil moisture was not from biases in the hydrology model.

3.3 Discrimination formulations: implications for model development

The *limited* and *unlimited model* formulations tested in this study represented two approaches to account for nitrogen limitation within ecosystem models. The *limited nitrogen* formulation reduced photosynthesis, *after the main photosynthesis calculation*, so that the carbon allocated to growth was accommodated by available nitrogen. This *allocation downscaling* approach is common to a subset of models, for example, CLM (Thornton et al., 2007), DAYCENT (Parton et al., 2010) and ED2.1 (Medvigy et al., 2009). Another class of models limits photosynthesis based upon foliar nitrogen content and adjusts the photosynthetic capacity through nitrogen availability in the leaf though V_{cmax} (e.g. CABLE, GDAY, LPJ-GUESS, OCN, SDVGM, TECO, see Zaehle et al., 2014). These *foliar nitrogen* models are similar to the *unlimited nitrogen* formulation of CLM because the scaling of photosynthesis was taken into account in the V_{cmax} scaling methodology (see discussion in section 2.1.2 and 2.4), *prior to the photosynthesis calculation*. In general, there were no categorical differences in behavior between these two classes of models during CO_2 manipulation experiments held at Duke forest and ORNL (Zaehle et al., 2014). CLM 4.0 was one of the few models in that study to consistently underestimate the NPP response to an increase of atmospheric CO_2 due to nitrogen limitation, however this finding was attributed to a lower initial supply of nitrogen.

The *unlimited nitrogen* formulation described in our study is a simplified foliar nitrogen model, in that, all of the information about nitrogen limitation is incorporated within the V_{cmax} downscaling approach. A more versatile approach would link a dynamic nitrogen cycle directly with the calculation of V_{cmax}. This capability is currently being developed within CLM (Ghimire et al., in review) and future work should test its functionality.

Biogeosciences Discuss., doi:10.5194/bg-2016-73, 2016
Manuscript under review for journal Biogeosciences
Published: 22 March 2016
© Author(s) 2016. CC-BY 3.0 License.

The performance of the *unlimited nitrogen* formulation was nearly identical to the *no downregulation discrimination* formulation in terms of isotopic behavior despite the mechanistic differences. The *no downregulation discrimination* formulation included nitrogen limitation within the bulk carbon behavior but ignored the impact of f_{dreg} upon discrimination behavior. The relative high simulation skill with this formulation implied that the 'potential' GPP linked to A_n, was a more effective predictor of discrimination behavior than the 'downscaled' GPP, which is linked to $A_n * (1\text{-}f_{dreg})$ (equation 9). There are several potential explanations for an unrealistically large value of f_{dreg}. First this could indicate that the V_{cmax} parameter was too large, thereby requiring a large f_{dreg} to compensate. As noted in Section (3.1) the default temperate evergreen V_{cmax25} was ~62 µmol m^{-2} s^{-1}, much larger than what was found based on literature reviews (Monson et al., 2005; Tomaszewski and Sievering, 2007) . We found to match the observed GPP we had to impose f_{dreg} that had the same effect as reducing V_{cmax} (Figure S1) to values of 51 and 34 µmol m^{-2} s^{-1} for the *limited nitrogen* and *unlimited nitrogen* formulations respectively. Alternatively, it could be that there are physiological processes that are acting to reduce nitrogen limitation (e.g. nitrogen storage pools or transient carbon storage as non-structural carbohydrates), or that the current measurement techniques are underestimating GPP due to biases within the flux partitioning methods.

3.4 Disequilibrium, possible explanations of mismatch

Carbon cycle models (e.g. Fung et al., 1997) indicate that the steady decrease of δ_{atm} (Suess effect, Fig. 1) should lead to a positive disequilibrium between land surface processes ($\delta^{13}C$ difference between GPP and ER, Eq. 12). This is because the δ_{GPP} reflects the most recent ($\delta^{13}C$ depleted) state of the atmosphere, whereas the δ_{ER} reflects carbon (e.g. soil carbon) assimilated from an older ($\delta^{13}C$ enriched) atmosphere. This positive disequilibrium pattern promoted by the Suess effect was consistent with all CLM formulations for this study with an annual average disequilibrium of 0.8 ‰. In contrast, a negative disequilibrium (-0.6 ‰) was identified at Niwot Ridge based upon observations (Bowling et al. 2014) as well as in other forests (Flanagan et al., 2012; Wehr and Saleska, 2015; Wingate et al., 2010). Bowling et al. (2014) hypothesized several reasons for this: 1) a strong seasonal stomatal response to atmospheric humidity, 2) decreased photosynthetic discrimination associated with CO_2 fertilization, 3) decreased photosynthetic discrimination associated with multi-decadal warming and increased VPD, and 4) post-photosynthetic discrimination. We evaluated the first three hypotheses within the context of the CLM simulations.

Biogeosciences Discuss., doi:10.5194/bg-2016-73, 2016
Manuscript under review for journal Biogeosciences
Published: 22 March 2016
© Author(s) 2016. CC-BY 3.0 License.

The model results suggest a seasonal variation of discrimination that is a function of both VPD and A_n. The simulated seasonal range in discrimination (Figure 7; Figure S3) varied by approximately 2 ‰, and this range in seasonal discrimination could contribute to a negative disequilibrium provided specific timing of assimilation, assimilate storage and respiration not currently considered in the model. For example, if a significant portion of photosynthetic assimilation was stored during the spring with relatively high discrimination, and then respired during the summer, the net effect would deplete the δ_{ER} and thereby promote negative disequilibrium during the summer months when discrimination is lower. Theoretically, this could be achieved by explicitly including carbohydrate storage pools within CLM. Isotopic tracer studies have shown assimilated carbon can exist for weeks to months within the vegetation and soil before it is finally respired (Epron et al., 2012; Hogberg et al., 2008). Although carbon storage pools are included in CLM, their allocation is almost always instantaneous for evergreen systems and could not provide the isotopic effect described above.

The CO_2 fertilization effect tends to favor photosynthesis in plants and has been shown to simultaneously increase WUE and decrease stomatal conductance as inferred from $\delta^{13}C$ in tree rings (Frank et al., 2015; Flanagan et al., 2012; Wingate et al., 2010). In general a decrease in stomatal conductance and increase in WUE is associated with a decrease in C3 discrimination (Farquhar et al., 1982), which opposes the disequilibrium trend imposed by the Suess effect. The model simulation agrees with both these trends in WUE and stomatal conductance, yet simulates an *increase* in discrimination (Figure 5; Figure 6), which reinforces the Suess effect pattern upon disequilibrium. Although this appears to be a mismatch between forest processes and model performance the model is operating within the limits of the discrimination parameterization (Eq. 17) in which the magnitude of photosynthetic discrimination is inversely proportional to the iWUE, but is also proportional to atmospheric CO_2 (see section 3.2.1).

A multi-decadal decrease in photosynthetic discrimination may also result from change in climate. Meteorological measurements at Niwot Ridge during the last several decades generally support conditions of higher VPD based upon a warming trend from an average annual temperature of 1.1 ^{o}C in the 1980's to 2.7 ^{o}C in the 2000's (Mitton and Ferrenberg, 2012) and no overall trend in precipitation. It is possible that a multi-decadal trend in increasing VPD contributed to multi-decadal weakening in photosynthetic discrimination given the observed (Bowling et al., 2014) and modelled (Figure 9) correlation between Δ_{canopy} and VPD. The model meteorology only included the years 1998-2013 and did not include the rapid

Biogeosciences Discuss., doi:10.5194/bg-2016-73, 2016
Manuscript under review for journal Biogeosciences
Published: 22 March 2016
© Author(s) 2016. CC-BY 3.0 License.

warming after the 1980's. It is unclear whether, if the full period of warming were to be included in the simulation, the simulated discrimination response to VPD would be enough to counter the Suess effect and lead to negative disequilibrium. Still, there is evidence that the model is overestimating contemporary discrimination (Section 3.4) and the exclusion of the full multi-decadal shift in VPD could be a significant reason why.

Finally, post-photosynthetic discrimination processes are likely to impact the magnitude and sign of the isotopic disequilibrium (Bowling et al., 2008; Brüggemann et al., 2011) at multiple temporal scales. None of these isotopic processes are currently modelled within CLM 4.5, so at present the model cannot be used to examine them.

4 Conclusions

This study provides a rigorous test of the representation of C isotope discrimination within the highly mechanistic terrestrial carbon model CLM. Special attention was paid to provide an accurate set of boundary conditions to isolate the isotopic performance including 1) customized atmospheric CO_2 and δ_{atm} time series, 2) customized model initialization procedure, and 3) empirical V_{cmax} calibration procedure. Once the model satisfactorily represented observed carbon exchange, water exchange, and biomass growth, it was successful at simulating several aspects of isotope behavior.

CLM was able to accurately simulate $\delta^{13}C$ in leaf and stem biomass and the seasonal cycle in Δ_{canopy}. This performance could only be achieved, however, if V_{cmax} were calibrated in such a way to mimic the functionality of a foliar nitrogen model by accounting for nitrogen limitation *prior* to photosynthesis. With the traditional *nitrogen limited* approach, in which the nitrogen limitation occurs *after* photosynthesis and the c_i/c_a is influenced by this limitation but the stomatal conductance is not, the model tended to overestimate the magnitude of photosynthetic discrimination, and eliminated the observed seasonal weakening of Δ_{canopy}. Although the overestimation of photosynthetic discrimination could likely be corrected with adjustments to the stomatal conductance parameterization, the seasonal trend was inherent to the model. Thus our results suggest that shifting nitrogen controls either before photosynthesis through a reduction in $V_{cmax,}$ or entirely after the photosynthetic process such that nitrogen constraints have no effect on discrimination, are more consistent with the isotopic observations than the current model formulation.

Although the *unlimited nitrogen* formulation was able to match observed $\delta^{13}C$ of biomass and seasonal patterns in discrimination, it still overestimated the contemporary magnitude of

Biogeosciences Discuss., doi:10.5194/bg-2016-73, 2016
Manuscript under review for journal Biogeosciences
Published: 22 March 2016
© Author(s) 2016. CC-BY 3.0 License.

discrimination (2006-2012). Future work should identify whether this overestimation was a result of parameterization (stomatal slope), exclusion of multi-decadal shifts in VPD, or limitations in the representation of stomatal conductance (Ball-Berry model).

The model attributed most of the range in seasonal discrimination to variation in net assimilation rate (A_n) followed by variation in VPD, with little to no impact from soil moisture. The model suggested that A_n drove the seasonal range in discrimination (across-month variation) whereas VPD drove the inter-annual variation during the summer months. This finding suggests that to simulate multi-decadal trends in photosynthetic discrimination, response to assimilation rate and VPD must be well represented within the model.

The model simulated a positive disequilibrium that was driven by both the Suess effect, and increased photosynthetic discrimination from CO_2 fertilization. It is possible that the negative disequilibrium that was inferred from observations (Bowling et al., 2014) was driven from the impacts of climate change and/or post-photosynthetic discrimination – not considered in this version of the model. Future work should quantify the impact of this multi-decadal warming and post-photosynthetic discrimination processes upon disequilibrium.

The model simulated a consistent increase in water-use efficiency as a response to CO_2 fertilization and decrease in stomatal conductance. The model simulated an increase in WUE despite an increase in discrimination, however C3 plants typically express the opposite trends (increase in WUE, decrease in discrimination). Although CLM includes parameterization that promotes an increase in WUE with a decrease in discrimination, this trend was likely neutralized by other environmental variables (e.g. increase in c_a).

Initial indications are that $\delta^{13}C$ isotope data can bring additional constraint to model parameterization beyond what traditional flux tower measurements of carbon, water exchange, and biomass measurements. The isotope measurements suggested a stomatal conductance value generally lower than what was consistent with the flux tower measurements. Unexpectedly, the isotopes also provided guidance upon model formulation related to nitrogen limitation. The success of our empirical approach to account for nutrient limitation within the V_{cmax} parameterization, suggests that additional testing of foliar nitrogen models are worthwhile.

Biogeosciences Discuss., doi:10.5194/bg-2016-73, 2016
Manuscript under review for journal Biogeosciences
Published: 22 March 2016
© Author(s) 2016. CC-BY 3.0 License.

Acknowledgements

This research was supported by the U.S. Department of Energy, Office of Science, Office of Biological and Environmental Research, Terrestrial Ecosystem Science Program under Award Number DE-SC0010625. Thank you to Sean Burns and Peter Blanken for sharing flux tower and meteorological data from Niwot Ridge. Thank you to those at NOAA who provided the atmospheric flask data from Niwot Ridge including Bruce Vaughn, Ed Dlugokencky, the INSTAAR Stable Isotope Lab and NOAA GMD. A special thanks to Keith Lindsay at NCAR for providing global CESM output to help improve the discussion of model behavior. The support and resources from the Center for High Performance Computing at the University of Utah are gratefully acknowledged.

Biogeosciences Discuss., doi:10.5194/bg-2016-73, 2016
Manuscript under review for journal Biogeosciences
Published: 22 March 2016
© Author(s) 2016. CC-BY 3.0 License.

References

Ainsworth, E. A. and Long, S. P.: What have we learned from 15 years of free-air CO2 enrichment (FACE)? A meta-analytic review of the responses of photosynthesis, canopy properties and plant production to rising CO2, New Phytol., 165(2), 351–372, doi:10.1111/j.1469-8137.2004.01224.x, 2005.

Andrews, S. F., Flanagan, L. B., Sharp, E. J. and Cai, T.: Variation in water potential, hydraulic characteristics and water source use in montane Douglas-fir and lodgepole pine trees in southwestern Alberta and consequences for seasonal changes in photosynthetic capacity, Tree Physiol., 32, 146–160, doi:10.1093/treephys/tpr136, 2012.

Aranibar, J. N., Berry, J. A., Riley, W. J., Pataki, D. E., Law, B. E. and Ehleringer, J. R.: Combining meteorology, eddy fluxes, isotope measurements, and modeling to understand environmental controls of carbon isotope discrimination at the canopy scale, Glob. Change Biol., 12(4), 710–730, 2006.

Arora, V. K., Boer, G. J., Friedlingstein, P., Eby, M., Jones, C. D., Christian, J. R., Bonan, G., Bopp, L., Brovkin, V., Cadule, P., Hajima, T., Ilyina, T., Lindsay, K., Tjiputra, J. F. and Wu, T.: Carbon-Concentration and Carbon-Climate Feedbacks in CMIP5 Earth System Models, J. Clim., 26(15), 5289–5314, doi:10.1175/jcli-d-12-00494.1, 2013.

Ballantyne, A. P., Miller, J. B. and Tans, P. P.: Apparent seasonal cycle in isotopic discrimination of carbon in the atmosphere and biosphere due to vapor pressure deficit, Glob. Biogeochem. Cycles, 24, GB3018, doi:10.1029/2009GB003623, 2010.

Ballantyne, A. P., Miller, J. B., Baker, I. T., Tans, P. P. and White, J. W. C.: Novel applications of carbon isotopes in atmospheric CO2: What can atmospheric measurements teach us about processes in the biosphere?, Biogeosciences, 8(10), 3093–3106, 2011.

Bauerle, W. L., Oren, R., Way, D. A., Qian, S. S., Stoy, P. C., Thornton, P. E., Bowden, J. D., Hoffman, F. M. and Reynolds, R. F.: Photoperiodic regulation of the seasonal pattern of photosynthetic capacity and the implications for carbon cycling, Proc. Natl. Acad. Sci. U. S. A., 109(22), 8612–8617, 2012.

Belmecheri, S., Maxwell, R. S., Taylor, A. H., Davis, K. J., Freeman, K. H. and Munger, W. J.: Tree-ring δ 13C tracks flux tower ecosystem productivity estimates in a NE temperate forest, Environ. Res. Lett., 9(7), 074011, doi:10.1088/1748-9326/9/7/074011, 2014.

Boisvenue, C. and Running, S. W.: Simulations show decreasing carbon stocks and potential for carbon emissions in Rocky Mountain forests over the next century, Ecol. Appl., 20(5), 1302–1319, 2010.

Bowling, D. R., Pataki, D. E. and Randerson, J. T.: Carbon isotopes in terrestrial ecosystem pools and CO2 fluxes, New Phytol., 178, 24–40, doi: 10.1111/j.1469–8137.2007.02342.x, 2008.

Bowling, D. R., Ballantyne, A. P., Miller, J. B., Burns, S. P., Conway, T. J., Menzer, O., Stephens, B. B. and Vaughn, B. H.: Ecological processes dominate the 13C land disequilibrium in a Rocky Mountain subalpine forest, Glob. Biogeochem. Cycles, 28(4), 2013GB004686, doi:10.1002/2013GB004686, 2014.

© Author(s) 2016. CC-BY 3.0 License.

Bradford, M. A., Fierer, N. and Reynolds, J. F.: Soil carbon stocks in experimental mesocosms are dependent on the rate of labile carbon, nitrogen and phosphorus inputs to soils, Funct. Ecol., 22(6), 964–974, doi:10.1111/j.1365-2435.2008.01404.x, 2008.

Braswell, B. H., Sacks, W. J., Linder, E. and Schimel, D. S.: Estimating diurnal to annual ecosystem parameters by synthesis of a carbon flux model with eddy covariance net ecosystem exchange observations, Glob. Change Biol., 11, 335–355, doi:10.1111/j.1365-2486.2005.00897.x, 2005.

Brüggemann, N., Gessler, A., Kayler, Z., Keel, S. G., Badeck, F., Barthel, M., Boeckx, P., Buchmann, N., Brugnoli, E., Esperschütz, J., Gavrichkova, O., Ghashghaie, J., Gomez-Casanovas, N., Keitel, C., Knohl, A., Kuptz, D., Palacio, S., Salmon, Y., Uchida, Y. and Bahn, M.: Carbon allocation and carbon isotope fluxes in the plant-soil-atmosphere continuum: a review, Biogeosciences, 8(11), 3457–3489, doi:10.5194/bg-8-3457-2011, 2011.

Collatz, G. J., Ball, J. T., Grivet, C. and Berry, J. A.: Regulation of stomatal conductances and transpiration a physiological model of canopy processes, Agric. For. Meteorol., 54, 107–136, 1991.

Desai, A. R., Moore, D. J. P., Ahue, W. K. M., Wilkes, P. T. V., De Wekker, S. F. J., Brooks, B. G., Campos, T. L., Stephens, B. B., Monson, R. K., Burns, S. P., Quaife, T., Aulenbach, S. M. and Schimel, D. S.: Seasonal pattern of regional carbon balance in the central Rocky Mountains from surface and airborne measurements, J. Geophys. Res., 116, G04009(4), doi:10.1029/2011JG001655, 2011.

Dlugokencky, E. J., Lang, P. M., Masarie, K. A., Crotwell, A. M. and Crotwell, M. J.: Atmospheric Carbon Dioxide Dry Air Mole Fractions from the NOAA ESRL Carbon Cycle Cooperative Global Air Sampling network, 1968-2014, Version: 2015-08-03, Path: ftp://aftp.cmdl.noaa.gov/data/trace_gases/co2/flask/surface/, 2015.

Ehleringer, J. R., Buchmann, N. and Flanagan, L. B.: Carbon isotope ratios in belowground carbon cycle processes, Ecol. Appl., 10(2), 412–422, 2000.

Epron, D., Bahn, M., Derrien, D., Lattanzi, F. A., Pumpanen, J., Gessler, A., Högberg, P., Maillard, P., Dannoura, M., Gérant, D. and Buchmann, N.: Pulse-labelling trees to study carbon allocation dynamics: a review of methods, current knowledge and future prospects, Tree Physiol., 32(6), 776–798, doi:10.1093/treephys/tps057, 2012.

Farquhar, G. D., von Caemmerer, S. and Berry, J. A.: A Biochemical Model of Photosynthetic CO2 Assimilation in Leaves of C3 Species, Planta, 149, 78–90, 1980.

Farquhar, G. D., O'Leary, M. H. and Berry, J. A.: On the relationship between carbon isotope discrimination and the intercellular carbon dioxide concentration in leaves, Aust. J. Plant Physiol., 9(2), 121–137, 1982.

Farquhar, G. D., Ehleringer, J. R. and Hubick, K. T.: Carbon isotope discrimination and photosynthesis, Annu. Rev. Plant Physiol. Plant Mol. Biol., 40, 503–537, 1989.

Flanagan, L. B., Cai, T., Black, T. A., Barr, A. G., McCaughey, J. H. and Margolis, H. A.: Measuring and modeling ecosystem photosynthesis and the carbon isotope composition of

© Author(s) 2016. CC-BY 3.0 License.

ecosystem-respired CO2 in three boreal coniferous forests, Agric. For. Meteorol., 153, 165–176, 2012.

Francey, R. J., Allison, C. E., Etheridge, D. M., Trudinger, C. M., Enting, I. G., Leuenberger, M., Langenfelds, R. L., Michel, E. and Steele, L. P.: A 1000-year high precision record of d13C in atmospheric CO2, Tellus, 51B, 170–193, 1999.

Frank, D. C., Poulter, B., Saurer, M., Esper, J., Huntingford, C., Helle, G., Treydte, K., Zimmermann, N. E., Schleser, G. H., Ahlström, A., Ciais, P., Friedlingstein, P., Levis, S., Lomas, M., Sitch, S., Viovy, N., Andreu-Hayles, L., Bednarz, Z., Berninger, F., Boettger, T., D'Alessandro, C. M., Daux, V., Filot, M., Grabner, M., Gutierrez, E., Haupt, M., Hilasvuori, E., Jungner, H., Kalela-Brundin, M., Krapiec, M., Leuenberger, M., Loader, N. J., Marah, H., Masson-Delmotte, V., Pazdur, A., Pawelczyk, S., Pierre, M., Planells, O., Pukiene, R., Reynolds-Henne, C. E., Rinne, K. T., Saracino, A., Sonninen, E., Stievenard, M., Switsur, V. R., Szczepanek, M., Szychowska-Krapiec, E., Todaro, L., Waterhouse, J. S. and Weigl, M.: Water-use efficiency and transpiration across European forests during the Anthropocene, Nat. Clim. Change, 5(6), 579–583, doi:10.1038/nclimate2614, 2015.

Franks, P. J., Adams, M. A., Amthor, J. S., Barbour, M. M., Berry, J. A., Ellsworth, D. S., Farquhar, G. D., Ghannoum, O., Lloyd, J., McDowell, N., Norby, R. J., Tissue, D. T. and von Caemmerer, S.: Sensitivity of plants to changing atmospheric CO2 concentration: From the geological past to the next century, New Phytol., 197(4), 1077–1094, 2013.

Friedlingstein, P., Cox, P. M., Betts, R. A., Bopp, L., von Bloh, W., Brovkin, V., Cadule, P., Doney, S. C., Eby, M., Fung, I. Y., Bala, G., John, J., Jones, C. D., Joos, F., Kato, T., Kawamiya, M., Knorr, W., Lindsay, K., Matthews, H. D., Raddatz, T., Rayner, P., Reick, C., Roeckner, E., Schnitzler, K.-G., Schnur, R., Strassmann, K., Weaver, A. J., Yoshikawa, C. and Zeng, N.: Climate-carbon cycle feedback analysis: Results from the C4MIP model intercomparison, J. Clim., 19, 3337–3353, 2006.

Fung, I. Y., Field, C. B., Berry, J. A., Thompson, M. V., Randerson, J. T., Malmstrom, C. M., Vitousek, P. M., Collatz, G. J., Sellers, P. J., Randall, D. A., Denning, A. S., Badeck, F. and John, J.: Carbon 13 exchanges between the atmosphere and biosphere, Glob. Biogeochem. Cycles, 11(4), 507–533, 1997.

Greenland, D.: The Climate of Niwot Ridge, Front Range, Colorado, U.S.A., Arct. Alp. Res., 21(4), 380–391, 1989.

Hogberg, P., Hogberg, M. N., Gottlicher, S. G., Betson, N. R., Keel, S. G., Metcalfe, D. B., Campbell, C., Schindlbacher, A., Hurry, V., Lundmark, T., Linder, S. and Nasholm, T.: High temporal resolution tracing of photosynthate carbon from the tree canopy to forest soil microorganisms, New Phytol., 177(1), 220–228, 2008.

Hu, J., Moore, D. J. P., Burns, S. P. and Monson, R. K.: Longer growing seasons lead to less carbon sequestration by a subalpine forest, Glob. Change Biol., 16(2), 771–783, doi:10.1111/j.1365-2486.2009.01967.x, 2010.

Katul, G. G., Ellsworth, D. S. and Lai, C.-T.: Modelling assimilation and intercellular CO2 from measured conductance: a synthesis of approaches, Plant Cell Environ., 23(12), 1313–1328, doi:10.1046/j.1365-3040.2000.00641.x, 2000.

© Author(s) 2016. CC-BY 3.0 License.

Keenan, T. F., Hollinger, D. Y., Bohrer, G., Dragoni, D., Munger, J. W., Schmid, H. P. and Richardson, A. D.: Increase in forest water-use efficiency as atmospheric carbon dioxide concentrations rise, Nature, 499(7458), 324–327, doi:10.1038/nature12291, 2013.

Kolari, P., Lappalainen, H. K., HäNninen, H. and Hari, P.: Relationship between temperature and the seasonal course of photosynthesis in Scots pine at northern timberline and in southern boreal zone, Tellus B, 59(3), 542–552, doi:10.1111/j.1600-0889.2007.00262.x, 2007.

Lasslop, G., Reichstein, M., Papale, D., Richardson, A., Arneth, A., Barr, A., Stoy, P. and Wohlfahrt, G.: Separation of net ecosystem exchange into assimilation and respiration using a light response curve approach: critical issues and global evaluation, Glob. Change Biol., 16, 187–208, 2010.

Le Quéré, C., Moriarty, R., Andrew, R. M., Peters, G. P., Ciais, P., Friedlingstein, P., Jones, S. D., Sitch, S., Tans, P., Arneth, A., Boden, T. A., Bopp, L., Bozec, Y., Canadell, J. G., Chini, L. P., Chevallier, F., Cosca, C. E., Harris, I., Hoppema, M., Houghton, R. A., House, J. I., Jain, A. K., Johannessen, T., Kato, E., Keeling, R. F., Kitidis, V., Klein Goldewijk, K., Koven, C., Landa, C. S., Landschützer, P., Lenton, A., Lima, I. D., Marland, G., Mathis, J. T., Metzl, N., Nojiri, Y., Olsen, A., Ono, T., Peng, S., Peters, W., Pfeil, B., Poulter, B., Raupach, M. R., Regnier, P., Rödenbeck, C., Saito, S., Salisbury, J. E., Schuster, U., Schwinger, J., Séférian, R., Segschneider, J., Steinhoff, T., Stocker, B. D., Sutton, A. J., Takahashi, T., Tilbrook, B., van der Werf, G. R., Viovy, N., Wang, Y.-P., Wanninkhof, R., Wiltshire, A. and Zeng, N.: Global carbon budget 2014, Earth Syst. Sci. Data, 7(1), 47–85, doi:10.5194/essd-7-47-2015, 2015.

Leuning, R.: A critical appraisal of a combined stomatal-photosynthesis model for C3 plants, Plant Cell Environ., 18(4), 339–355, doi:10.1111/j.1365-3040.1995.tb00370.x, 1995.

Mao, J., Ricciuto, D. M., Thornton, P. E., Warren, J. M., King, A. W., Shi, X., Iversen, C. M. and Norby, R. J.: Evaluating the Community Land Model in a pine stand with shading manipulations and ¹³CO₂ labeling, Biogeosciences, 13(3), 641–657, doi:10.5194/bg-13-641-2016, 2016.

Martinelli, L. A., Almeida, S., Brown, I. F., Moreira, M. Z., Victoria, R. L., Sternberg, L. S. L., Ferreira, C. A. C. and Thomas, W. W.: Stable carbon isotope ratio of tree leaves, boles and fine litter in a tropical forest in Rondonia, Brazil, Oecologia, 114(2), 170–179, 1998.

McDowell, N. G., Allen, C. D. and Marshall, L.: Growth, carbon-isotope discrimination, and drought-associated mortality across a Pinus ponderosa elevational transect, Glob. Change Biol., 16(1), 399–415, 2010.

Medvigy, D., Wofsy, S. C., Munger, J. W., Hollinger, D. Y. and Moorcroft, P., R.: Mechanistic scaling of ecosystem function and dynamics in space and time: Ecosystem Demography model version 2, J. Geophys. Res.-Biogeosciences, 114, G01002, doi:10.1029/2008JG000812, 2009.

Mitton, J. . and Ferrenberg, S. M.: Mountain pine beetle develops an unprecedented summer generation in response to climate warming, Am. Nat., 179(5), 1–9, 2012.

Monson, R. K., Turnipseed, A. A., Sparks, J. P., Harley, P. C., Scott-Denton, L. E., Sparks, K. and Huxman, T. E.: Carbon sequestration in a high-elevation, subalpine forest, Glob. Change Biol., 8, 459–478, 2002.

© Author(s) 2016. CC-BY 3.0 License.

Monson, R. K., Sparks, J. P., Rosentiel, T. N., Scott-Denton, L. E., Huxman, T. E., Harley, P. C., Turnipseed, A. A., Burns, S. P., Backlund, B. and Hu, J.: Climatic influences on net ecosystem CO2 exchange during the transition from wintertime carbon source to springtime carbon sink in a high-elevation, subalpine forest, Oecologia, 146, 130–147; doi:10.1007/s00424–005–0169–2, 2005.

Oleson et al.: Technical Description of version 4.5 of the Community Land Model (CLM), [online] Available from: http://www.cesm.ucar.edu/models/cesm1.2/clm/CLM45_Tech_Note.pdf, 2013.

Parton, W. J., Hanson, P. J., Swanston, C., Torn, M., Trumbore, S. E., Riley, W. and Kelly, R.: ForCent model development and testing using the Enriched Background Isotope Study experiment, J. Geophys. Res. Biogeosciences, 115(G4), G04001, doi:10.1029/2009JG001193, 2010.

Peñuelas, J., Canadell, J. G. and Ogaya, R.: Increased water-use efficiency during the 20th century did not translate into enhanced tree growth, Glob. Ecol. Biogeogr., 20(4), 597–608, doi:10.1111/j.1466-8238.2010.00608.x, 2011.

Reichstein, M., Falge, E., Baldocchi, D., Papale, D., Aubinet, M., Berbigier, P., Bernhofer, C., Buchmann, N., Gilmanov, T., Granier, A., Grunwald, T., Havrankova, K., Ilvesniemi, H., Janous, D., Knohl, A., Laurila, T., Lohila, A., Loustau, D., Matteucci, G., Meyers, T., Miglietta, F., Ourcival, J. M., Pumpanen, J., Rambal, S., Rotenberg, E., Sanz, M., Tenhunen, J., Seufert, G., Vaccari, F., Vesala, T., Yakir, D. and Valentini, R.: On the separation of net ecosystem exchange into assimilation and ecosystem respiration: review and improved algorithm, Glob. Change Biol., 11(9), 1424–1439, 2005.

Ricciuto, D. M., Davis, K. J. and Keller, K.: A Bayesian calibration of a simple carbon cycle model: The role of observations in estimating and reducing uncertainty, Glob. Biogeochem. Cycles, 22, GB2030, doi:10.1029/2006GB002908, 2008.

Ricciuto, D. M., King, A. W., Dragoni, D. and Post, W. M.: Parameter and prediction uncertainty in an optimized terrestrial carbon cycle model: Effects of constraining variables and data record length, J. Geophys. Res. Biogeosciences, 116(G1), G01033, doi:10.1029/2010JG001400, 2011.

Richardson, A. D., Williams, M., Hollinger, D. Y., Moore, D. J. P., Dail, D. B., Davidson, E. A., Scott, N. A., Evans, R. S., Hughes, H., Lee, J. T., Rodrigues, C. and Savage, K.: Estimating parameters of a forest ecosystem C model with measurements of stocks and fluxes as joint constraints, Oecologia, 164(1), 25–40, 2010.

Roden, J. S. and Ehleringer, J. R.: Summer precipitation influences the stable oxygen and carbon isotopic composition of tree-ring cellulose in Pinus ponderosa, Tree Physiol., 27(4), 491–501, 2007.

Rubino, M., Etheridge, D. M., Trudinger, C. M., Allison, C. E., Battle, M. O., Langenfelds, R. L., Steele, L. P., Curran, M., Bender, M., White, J. W. C., Jenk, T. M., Blunier, T. and Francey, R. J.: A revised 1000 year atmospheric δ13C-CO2 record from Law Dome and South Pole, Antarctica, J. Geophys. Res. Atmospheres, 118(15), 8482–8499, doi:10.1002/jgrd.50668, 2013.

© Author(s) 2016. CC-BY 3.0 License.

Saurer, M., Siegwolf, R. T. W. and Schweingruber, F. H.: Carbon isotope discrimination indicates improving water-use efficiency of trees in northern Eurasia over the last 100 years, Glob. Change Biol., 10(12), 2109–2120, doi:10.1111/j.1365-2486.2004.00869.x, 2004.

Saurer, M., Spahni, R., Frank, D. C., Joos, F., Leuenberger, M., Loader, N. J., McCarroll, D., Gagen, M., Poulter, B., Siegwolf, R. T. W., Andreu-Hayles, L., Boettger, T., Dorado Liñán, I., Fairchild, I. J., Friedrich, M., Gutierrez, E., Haupt, M., Hilasvuori, E., Heinrich, I., Helle, G., Grudd, H., Jalkanen, R., Levanič, T., Linderholm, H. W., Robertson, I., Sonninen, E., Treydte, K., Waterhouse, J. S., Woodley, E. J., Wynn, P. M. and Young, G. H. F.: Spatial variability and temporal trends in water-use efficiency of European forests, Glob. Change Biol., 20(12), 3700–3712, doi:10.1111/gcb.12717, 2014.

Schaeffer, S. M., Miller, J. B., Vaughn, B. H., White, J. W. C. and Bowling, D. R.: Long-term field performance of a tunable diode laser absorption spectrometer for analysis of carbon isotopes of CO2 in forest air, Atmospheric Chem. Phys., 8, 5263–5277, 2008.

Schimel, D. T., Kittel, G. F., Running, S., Monson, R., Turnispeed, A. and Anderson, D.: Carbon sequestration studied in western U.S. mountains, Eos Trans AGU, 83(40), 445–449, 2002.

Scott-Denton, L. E., Sparks, K. L. and Monson, R. K.: Spatial and temporal controls of soil respiration rate in a high-elevation, subalpine forest, Soil Biol. Biochem., 35, 525–534, 2003.

Sellers, P. J., Randall, D. A., Collatz, G. J., Berry, J. A., Field, C. B., Dazlich, D. A., Zhang, C., Collelo, G. D. and Bounoua, L.: A revised land surface parameterization (SiB2) for atmospheric GCMs. Part I: Model formulation, J. Clim., 9(4), 676–705, 1996.

Thornton, P. E. and Rosenbloom, N. A.: Ecosystem model spin-up: Estimating steady state conditions in a coupled terrestrial carbon and nitrogen cycle model, Ecol. Model., 189(1–2), 25–48, doi:10.1016/j.ecolmodel.2005.04.008, 2005.

Thornton, P. E., Law, B. E., Gholz, H. L., Clark, K. L., Falge, E., Ellsworth, D. S., Golstein, A. H., Monson, R. K., Hollinger, D., Falk, M., Chen, J. and Sparks, J. P.: Modeling and measuring the effects of disturbance history and climate on carbon and water budgets in evergreen needleleaf forests, Agric. For. Meteorol., 113(1-4), 185–222, 2002.

Thornton, P. E., Lamarque, J.-F., Rosenbloom, N. A. and Mahowald, N. M.: Influence of carbon-nitrogen cycle coupling on land model response to CO2 fertilization and climate variability, Glob. Biogeochem. Cycles, 21, GB4018, doi:10.1029/2006GB002868, 2007.

Trolier, M., White, J. W. C., Tans, P. P., Masarie, K. A. and Gemery, P. A.: Monitoring the isotopic composition of atmospheric CO2: Measurements from the NOAA Global Air Sampling Network, J. Geophys. Res.-Atmospheres, 101(D20), 25,897–25,916, 1996.

Wehr, R. and Saleska, S. R.: An improved isotopic method for partitioning net ecosystem–atmosphere CO2 exchange, Agric. For. Meteorol., 214–215, 515–531, doi:10.1016/j.agrformet.2015.09.009, 2015.

White et al.: Parameterization and Sensitivity Analysis of the Biome-BGC Terrestrial Ecosystem Model: Net Primary Production Controls, [online] Available from: http://secure.ntsg.umt.edu/publications/2000/WTRN00/White_2000.pdf, 2000.

© Author(s) 2016. CC-BY 3.0 License.

White, J. W. C., Vaughn, B. H., Michel, S. E., University of Colorado and Institute of Arctic and Alpine Research (INSTAAR): Stable Isotopic Composition of Atmospheric Carbon Dioxide (13C and 18O) from the NOAA ESRL Carbon Cycle Cooperative Global Air Sampling Network, 1990-2014, Version: 2015-10-26, Path: ftp://aftp.cmdl.noaa.gov/data/trace_gases/co2c13/flask/, 2015.

Wingate, L., Ogee, J., Burlett, R., Bosc, A., Devaux, M., Grace, J., Loustau, D. and Gessler, A.: Photosynthetic carbon isotope discrimination and its relationship to the carbon isotope signals of stem, soil and ecosystem respiration, New Phytol., 188(2), 576–589, 2010.

Zaehle, S., Medlyn, B. E., De Kauwe, M. G., Walker, A. P., Dietze, M. C., Hickler, T., Luo, Y., Wang, Y.-P., El-Masri, B., Thornton, P., Jain, A., Wang, S., Warlind, D., Weng, E., Parton, W., Iversen, C. M., Gallet-Budynek, A., McCarthy, H., Finzi, A., Hanson, P. J., Prentice, I. C., Oren, R. and Norby, R. J.: Evaluation of 11 terrestrial carbon–nitrogen cycle models against observations from two temperate Free-Air CO2 Enrichment studies, New Phytol., 202(3), 803–822, doi:10.1111/nph.12697, 2014.

Zarter, C. R., Demmig-Adams, B., Ebbert, V., Adamska, I. and Adams, W. W.: Photosynthetic capacity and light harvesting efficiency during the winter-to-spring transition in subalpine conifers, New Phytol., 172(2), 283–292, doi:10.1111/j.1469-8137.2006.01816.x, 2006.

Zeng, X.: Global Vegetation Root Distribution for Land Modeling, J. Hydrometeorol., 2(5), 525–530, doi:10.1175/1525-7541(2001)002<0525:GVRDFL>2.0.CO;2, 2001.

Zeng, X. and Decker, M.: Improving the Numerical Solution of Soil Moisture–Based Richards Equation for Land Models with a Deep or Shallow Water Table, J. Hydrometeorol., 10(1), 308–319, doi:10.1175/2008JHM1011.1, 2009.

Biogeosciences Discuss., doi:10.5194/bg-2016-73, 2016
Manuscript under review for journal Biogeosciences
Published: 22 March 2016
© Author(s) 2016. CC-BY 3.0 License.

1 Table 1. List of symbols used.

Symbol	Description	Unit or Unit Symbol
α_{psn}	Fractionation factor (R_a/ R_{GPP})	dimensionless
β_t	Soil water stress parameter (BTRAN)	dimensionless
Δ_{canopy}	photosynthetic carbon isotope discrimination	‰
$\delta^{13}C$	$^{13}C/^{12}C$ isotope composition (relative to VPDB)	‰
δ_{atm}	$\delta^{13}C$ of atmospheric CO_2	‰
δ_{ER}	$\delta^{13}C$ of ecosystem respiration	‰
δ_{GPP}	$\delta^{13}C$ of net photosynthetic assimilation	‰
Γ_*	CO_2 compensation point	Pa
A_c	Enzyme-limiting rate of photosynthetic assimilation	μmol m^{-2} s^{-1}
A_j	Light-limiting rate of photosynthetic assimilation	μmol m^{-2} s^{-1}
A_p	Product-limiting rate of photosynthetic assimilation	μmol m^{-2} s^{-1}
A_n	net photosynthetic assimilation	μmol m^{-2} s^{-1}
$Resp_d$	Leaf-level dark respiration	μmol m^{-2} s^{-1}
a_{R25}	Specific activity of Rubisco at 25ºC	μmol g^{-1} Rubisco s^{-1}
b	Minimum stomatal conductance	μmol m^{-2} s^{-1}
CF_{alloc}	Actual carbon allocated to biomass (N-limited)	gC m^{-2} s^{-1}
CF_{av_alloc}	Maximum carbon available for allocation to biomass	gC m^{-2} s^{-1}
CF_{GPPpot}	Potential gross primary production (non N-limited)	gC m^{-2} s^{-1}
c_a	Atmospheric CO_2 pressure	Pa
c_i	Leaf intracellular CO_2 pressure	Pa
c_i*	Leaf intracellular CO_2 pressure, (N-limited)	Pa
c_s	Leaf surface CO_2 pressure	Pa
e_l	Saturation vapor pressure	Pa
e_s	Water vapor pressure at leaf surface	Pa
E_T	Leaf Transpiration	μmol m^{-2} s^{-1}
ER	Ecosystem respiration	μmol m^{-2} s^{-1}
GPP	Gross primary productivity (photosynthesis)	μmol m^{-2} s^{-1}
F_{LNR}	Fraction of leaf nitrogen within Rubisco	gN Rubisco g^{-1} N
F_{NR}	Total Rubisco mass per nitrogen mass within Rubisco	g Rubisco g^{-1} N Rubisco
f_{df}	V_{cmax} scaling factor	dimensionless
f_{dreg}	Nitrogen photosynthetic downregulation factor	dimensionless
g_b	Leaf boundary layer conductance	μmol m^{-2} s^{-1}
g_s	Leaf stomatal conductance	μmol m^{-2} s^{-1}
h_s	Leaf surface humidity	Pa Pa^{-1}
K_c	Michaelis-Menten constant	Pa
K_o	Michaelis-Menten constant	Pa
LE	Latent heat flux	W m^{-2}
m	Stomatal slope (Ball Berry conductance model)	dimensionless
Na	Leaf nitrogen concentration	gN m^{-2} leaf area
NEE	Net ecosystem exchange	μmol m^{-2} s^{-1}
NPP	Net primary production	μmol m^{-2} s^{-1}
o_i	O_2 atmospheric partial pressure	Pa
PFT	Plant functional type	N/A
P_{atm}	Atmospheric pressure	Pa
R_a	Isotopic ratio of canopy air	$^{13}C/^{12}C$

Biogeosciences Discuss., doi:10.5194/bg-2016-73, 2016
Manuscript under review for journal Biogeosciences
Published: 22 March 2016
© Author(s) 2016. CC-BY 3.0 License.

R_{GPP}	Isotopic ratio of net photosynthetic assimilation	$^{13}C/^{12}C$
R_{VPDB}	Isotopic ratio of Vienna Pee Dee Belemnite standard	$^{13}C/^{12}C$
r	Fraction of roots (for β_t)	dimensionless
V_{cmax25}	Maximum carboxylation rate at 25°C	μmol m^{-2} s^{-1}
V_{cmax}	Maximum carboxylation rate at leaf temperature	μmol m^{-2} s^{-1}
VPD	Vapor pressure deficit	Pa
w	Plant wilting factor (for β_t)	dimensionless
WUE	Water use efficiency, ground area basis	gC gH_20^{-1}
iWUE	Intrinsic water use efficiency, leaf area basis	gC gH_20^{-1}

1

Biogeosciences Discuss., doi:10.5194/bg-2016-73, 2016
Manuscript under review for journal Biogeosciences
Published: 22 March 2016
© Author(s) 2016. CC-BY 3.0 License.

Table 2. CLM 4.5 model formulation description based upon timing of nitrogen limitation. Pre-photosynthetic and post-photosynthetic nitrogen limitation are achieved through V_{cmax25} calibration (equation 15) and f_{dreg} (equation 7) respectively.

Formulation	Pre-Photosynthetic Nitrogen Limitation	Post-Photosynthetic Nitrogen Limitation	Impact on c_i/c_a & discrimination	Impact on stomatal conductance
Limited nitrogen (default)	Yes (weak)	Yes, $f_{dreg} > 0$	Yes	No
Unlimited nitrogen	Yes (strong)	No, $f_{dreg} = 0$	Yes	Yes
No downregulation discrimination	Yes (weak)	Yes, $f_{dreg} > 0$	No	No

Biogeosciences Discuss., doi:10.5194/bg-2016-73, 2016
Manuscript under review for journal Biogeosciences
Published: 22 March 2016
© Author(s) 2016. CC-BY 3.0 License.

1 Table 3. CLM 4.5 key parameter values for all model formulations

Parameter	Description	Value	Units
froot_leaf	new fine root C per new leaf C	0.5	gC gC^{-1}
froot_cn	fine root (C:N)	55	gC gN^{-1}
leaf_long	leaf longevity	5	years
leaf_cn	leaf (C:N)	50	gC gN^{-1}
lflitcn	leaf litter (C:N)	100	gC gN^{-1}
slatop	specific leaf area (top canopy)	0.007	m^2 gC^{-1}
stem_leaf	new stem C per new leaf C	2	gC gC^{-1}
mp	stomatal slope	9	
croot_stem	coarse root: stem allocation	0.3	gC gC^{-1}
deadwood_cn	dead wood (C:N)	500	gC gN^{-1}
livewood_cn	live wood (C:N)	50	gC gN^{-1}
flnr	fraction of leaf nitrogen within Rubisco enzyme	0.0509	gN gN^{-1}
decomp_depth_e_folding	controls soil decomposition rate with depth	20	m

2

3

Biogeosciences Discuss., doi:10.5194/bg-2016-73, 2016
Manuscript under review for journal Biogeosciences
Published: 22 March 2016
© Author(s) 2016. CC-BY 3.0 License.

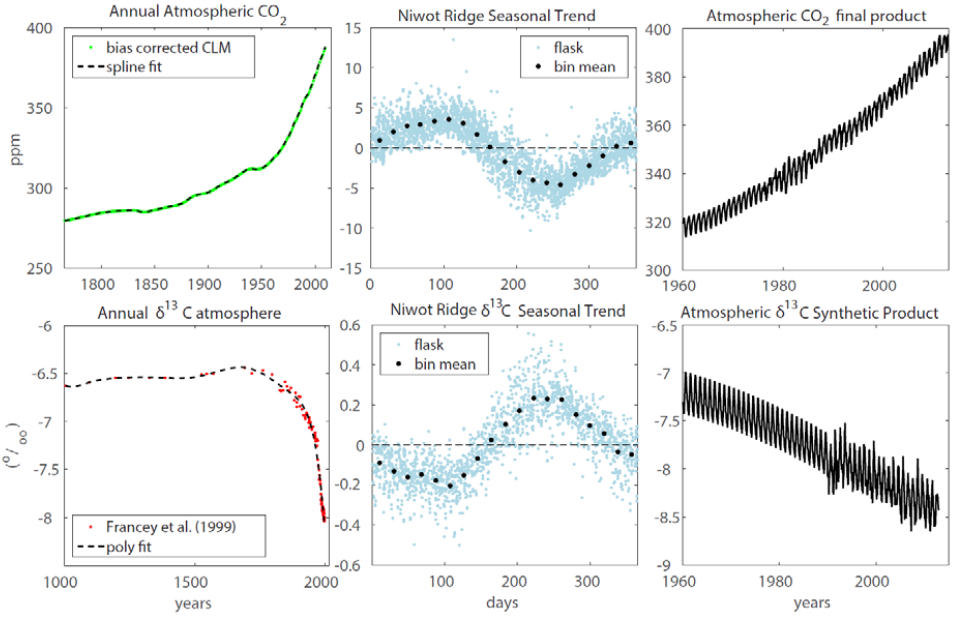

Figure 1. Niwot Ridge synthetic data product for atmospheric CO_2 concentration (c_a) (top row) and $\delta^{13}C$ of CO_2 (δ_{atm}) (bottom row). The final time series (right column) was used as a boundary condition for CLM, and created by combining the annual trends reported by Francey et al. (1999) adjusted for Niwot Ridge (left column) with the mean seasonal cycles measured at Niwot Ridge (middle column).

Biogeosciences Discuss., doi:10.5194/bg-2016-73, 2016
Manuscript under review for journal Biogeosciences
Published: 22 March 2016
© Author(s) 2016. CC-BY 3.0 License.

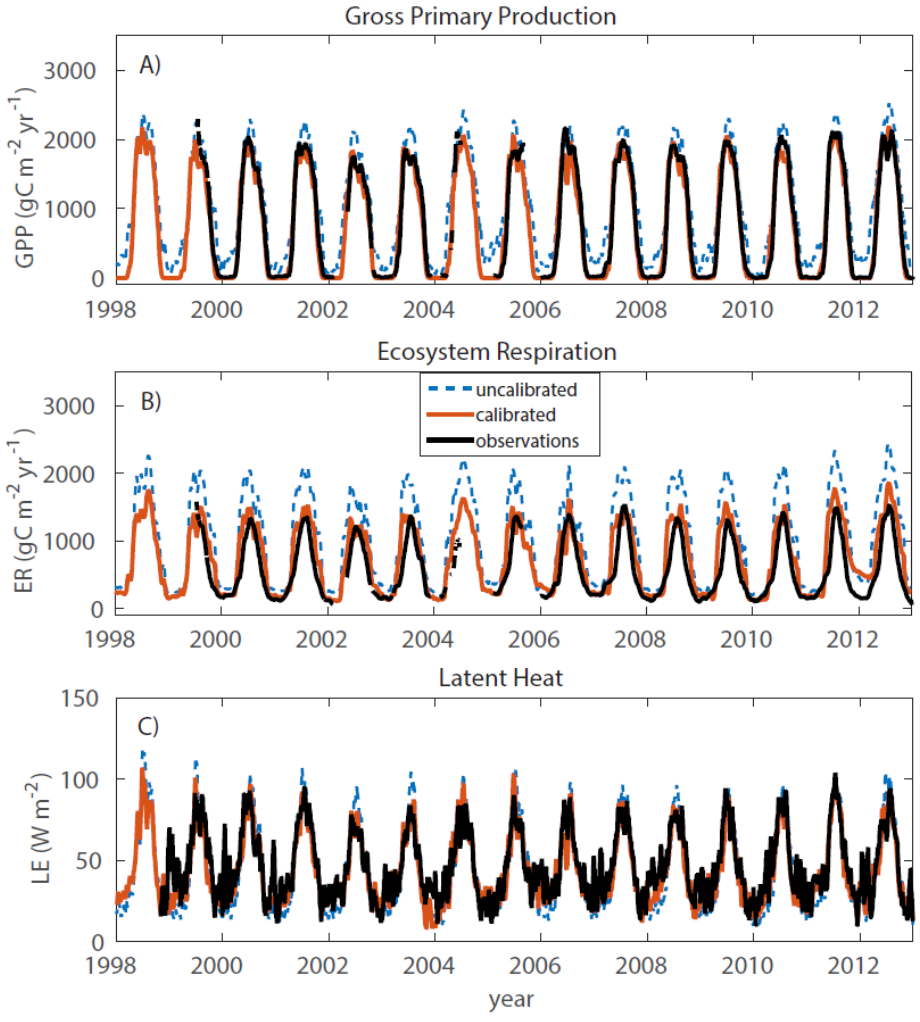

Figure 2. Simulated and observed land-atmosphere fluxes of A) gross primary production (GPP) B) ecosystem respiration (ER) and C) latent heat (LE) for the *limited nitrogen* simulation. The 'observations' are taken from the Ameriflux L2 processed eddy covariance flux tower data, partitioned into GPP and ER using the method of Reichstein et al. (2005). The *uncalibrated* simulation represents the CLM simulation without V_{cmax} scaling and the *calibrated* simulation represents the CLM run using the V_{cmax} scaling approach.

Biogeosciences Discuss., doi:10.5194/bg-2016-73, 2016
Manuscript under review for journal Biogeosciences
Published: 22 March 2016
© Author(s) 2016. CC-BY 3.0 License.

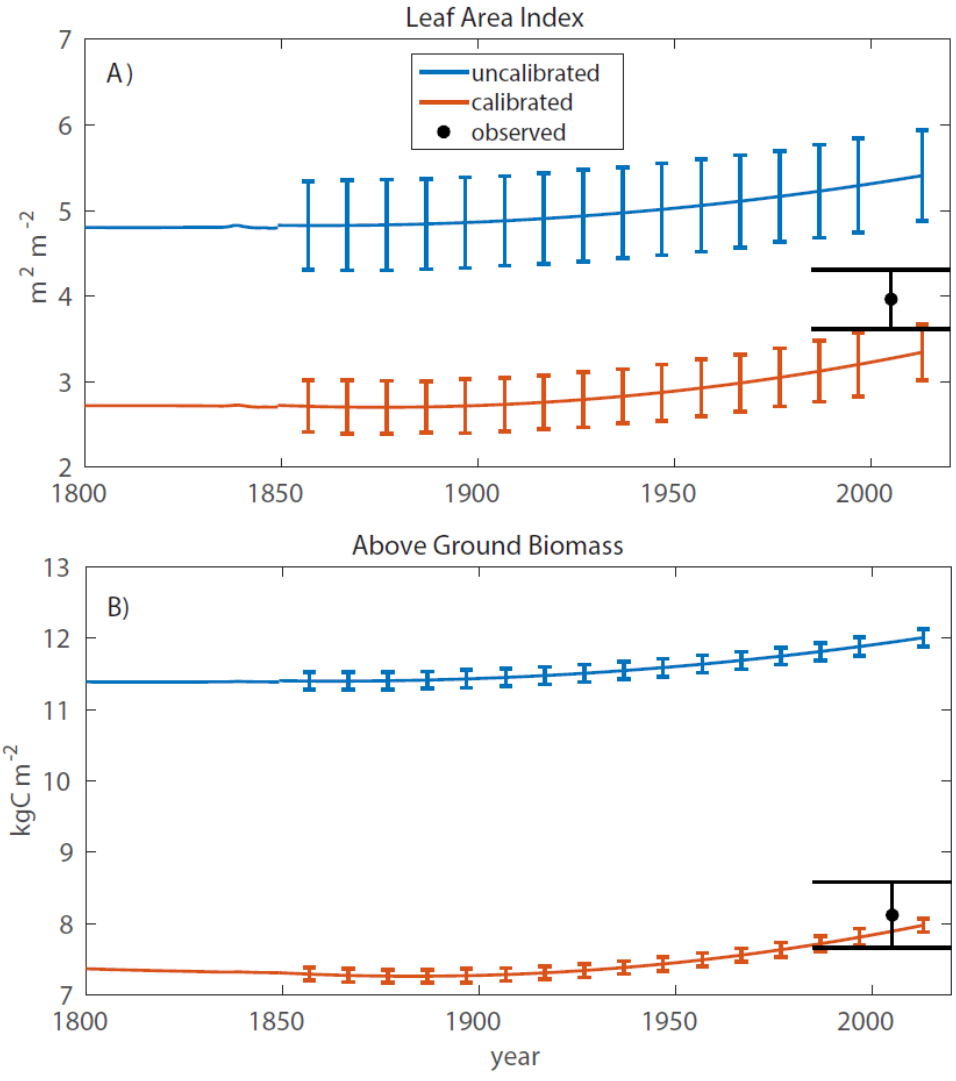

Figure 3. Simulation of A) leaf area index and B) above ground biomass for both uncalibrated and calibrated (V_{cmax} downscaled, *limited nitrogen*) simulation. Observations are from Bradford et al. (2008) with uncertainty bars representing standard error. Uncertainty bars on simulated runs represent 95% confidence of biomass variation as a result of cycling the site level meteorology observations.

Biogeosciences Discuss., doi:10.5194/bg-2016-73, 2016
Manuscript under review for journal Biogeosciences
Published: 22 March 2016
© Author(s) 2016. CC-BY 3.0 License.

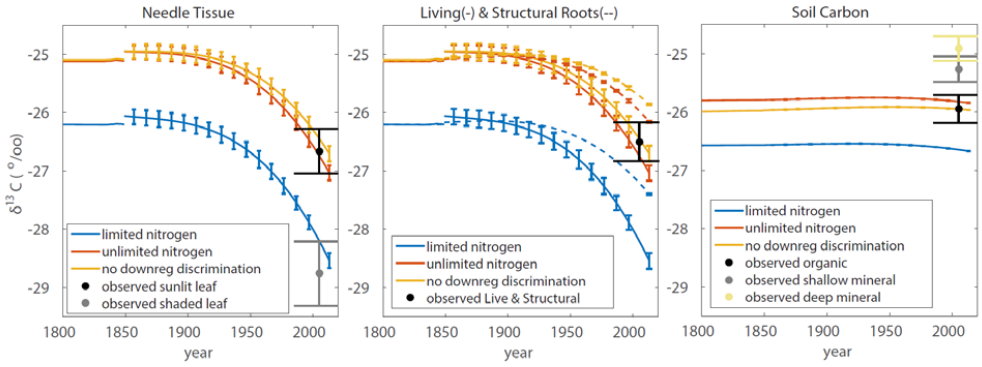

Figure 4. Simulation of $\delta^{13}C$ of bulk needle tissue, bulk roots and bulk soil carbon. A description of model formulations are provided in Table (2). Uncertainty bars for simulations represent 95% confidence intervals of $\delta^{13}C$ variation as a result of cycling the site level meteorology observations. The observed values are from Schaeffer et al. (2008) with uncertainty bars representing standard error. Solid lines and dashed lines in middle panel represent living roots and structural roots respectively.

Biogeosciences Discuss., doi:10.5194/bg-2016-73, 2016
Manuscript under review for journal Biogeosciences
Published: 22 March 2016
© Author(s) 2016. CC-BY 3.0 License.

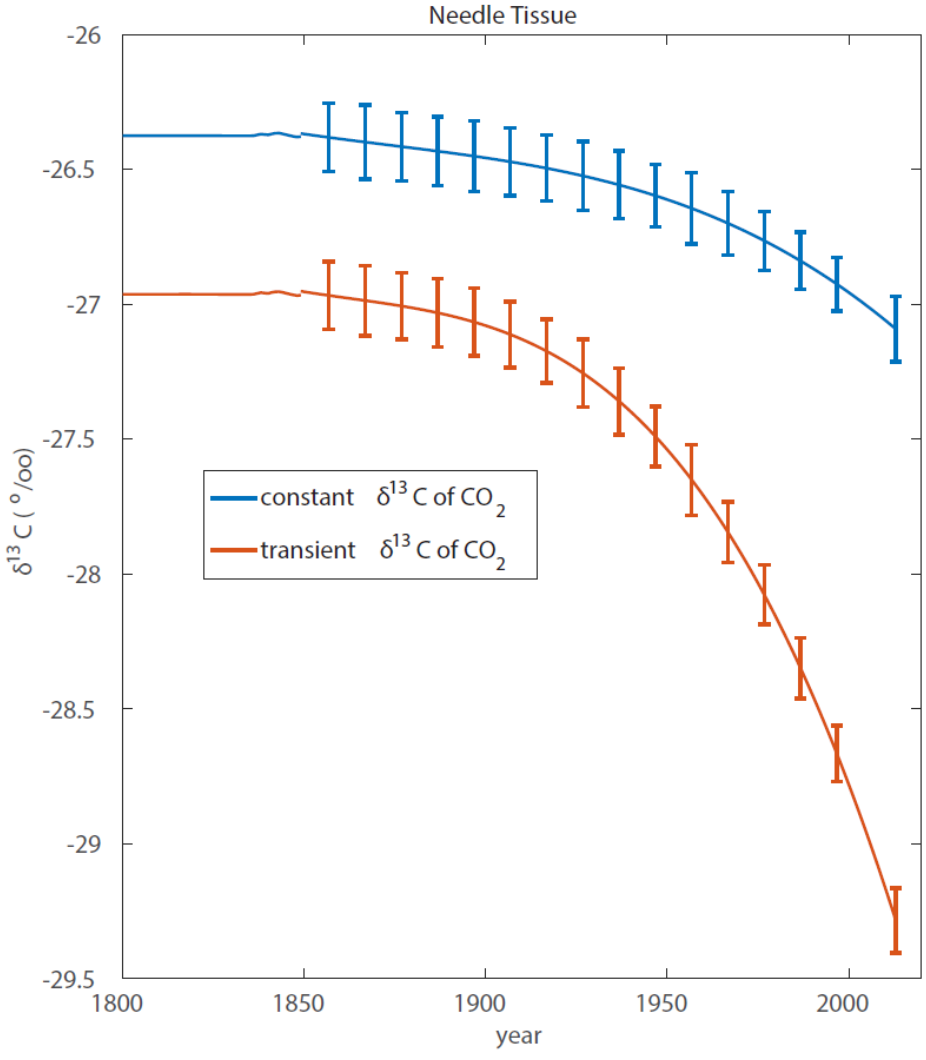

Figure 5. Simulation of $\delta^{13}C$ of needle tissue using the *limited nitrogen* (default) CLM run. In the *constant $\delta^{13}C$ of CO2 (δ_{atm})* simulation the model boundary condition was -6 ‰, whereas the *transient* δ_{atm} simulation varied over time (Figure 1).

Biogeosciences Discuss., doi:10.5194/bg-2016-73, 2016
Manuscript under review for journal Biogeosciences
Published: 22 March 2016
© Author(s) 2016. CC-BY 3.0 License.

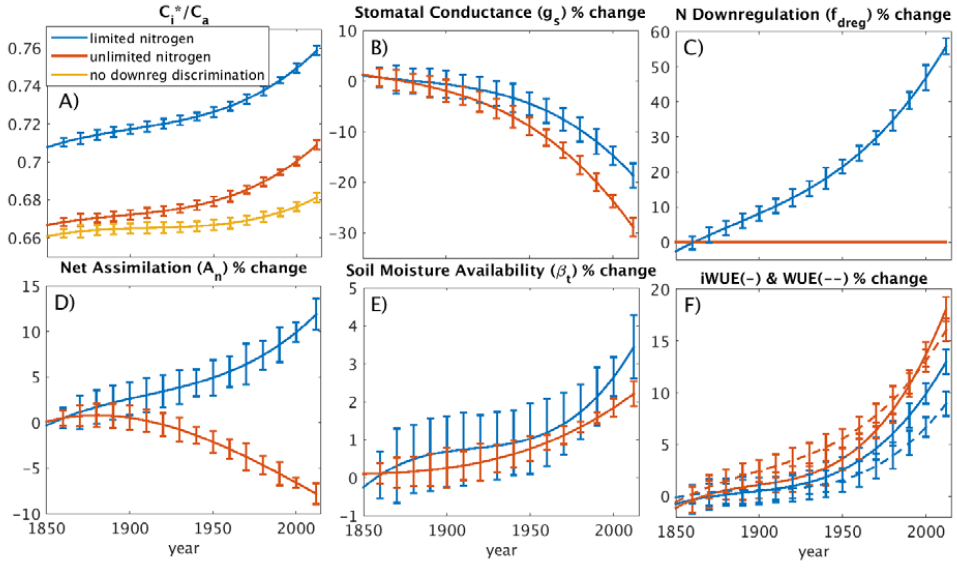

Figure 6. Diagnostic model variables that explain the discrimination trends (Figure 4) for the three model formulations as described in Table (2) for A) c_i^*/c_a, B) g_s, C) f_{dreg}, D) A_n, E) β_t, and F) the water use efficiency (WUE) and intrinsic water use efficiency (iWUE). Where the *no downregulation discrimination* simulation is not shown, it was identical to the *limited nitrogen* simulation. Uncertainty bars represent 95 % confidence intervals of diagnostic variable variation as a result of cycling the site level meteorology observations. The dashed lines represent WUE and the solid lines represent iWUE in panel F.

Biogeosciences Discuss., doi:10.5194/bg-2016-73, 2016
Manuscript under review for journal Biogeosciences
Published: 22 March 2016
© Author(s) 2016. CC-BY 3.0 License.

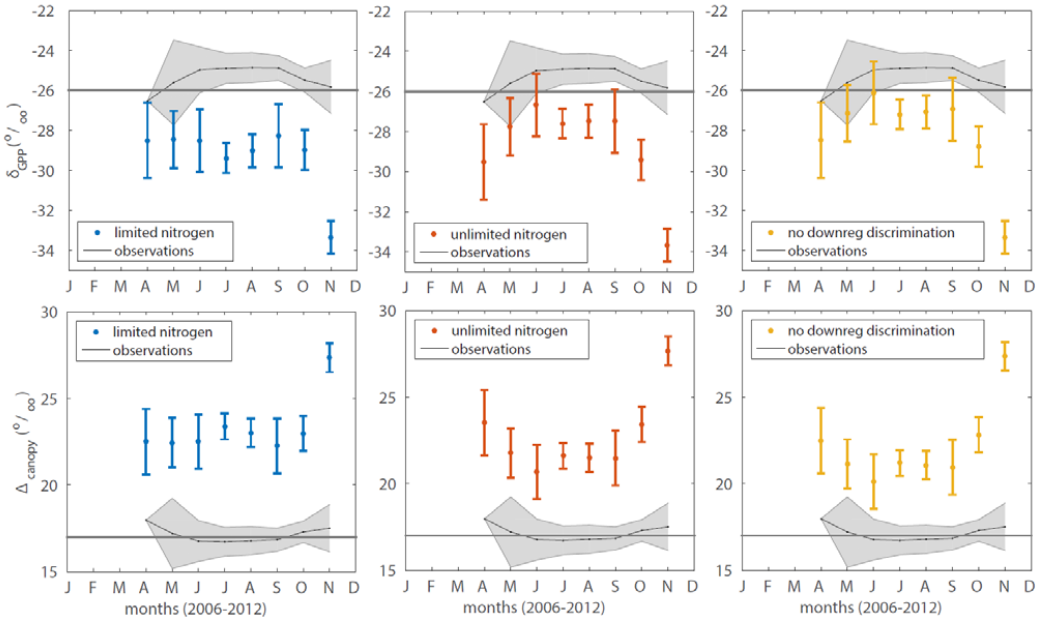

Figure 7. The seasonal pattern of photosynthetic discrimination as shown through δ_{GPP} (top row) and Δ_{canopy} (bottom row). Uncertainty bars represent 95% confidence bounds of simulated monthly average values from 2006-2012. Gray-shaded observation bounds represent 95% confidence intervals of 'observed' monthly average values based upon isotopic mixing model using Reichstein et al. (2005) partitioning of net ecosystem exchange flux described by (Bowling et al. 2014). The horizontal lines at $\delta^{13}C$ of -26 ‰ (top row) and 17 ‰ (bottom row) are included for reference.

Biogeosciences Discuss., doi:10.5194/bg-2016-73, 2016
Manuscript under review for journal Biogeosciences
Published: 22 March 2016
© Author(s) 2016. CC-BY 3.0 License.

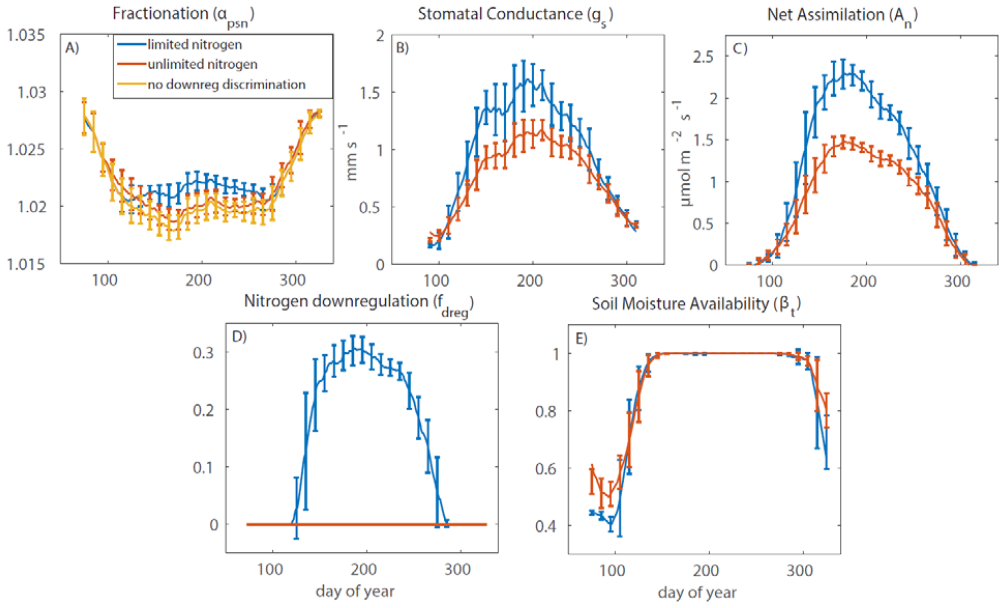

Figure 8. The seasonal pattern of discrimination (panel A) and diagnostic variables that explain the discrimination pattern in Figure (7). The individual tiles provide behavior from days 75-325 for A) α_{psn}, B) g_s, C) A_n, D) f_{dreg}, and E) β_t. Where the *no downregulation discrimination* model simulation is not shown, it is identical to the *limited nitrogen* simulation. Uncertainty bars represent 95 % confidence intervals of inter-annual variation from 2006-2012.

Biogeosciences Discuss., doi:10.5194/bg-2016-73, 2016
Manuscript under review for journal Biogeosciences
Published: 22 March 2016
© Author(s) 2016. CC-BY 3.0 License.

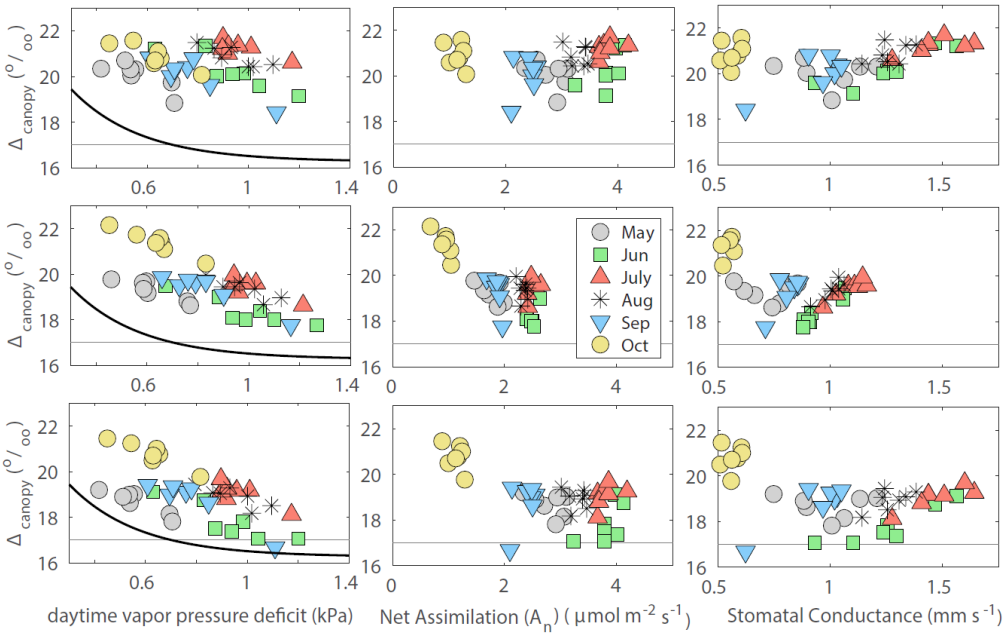

Figure 9. Relationship between monthly average photosynthetic discrimination and monthly average vapor pressure deficit (1st column), A_n (2nd column) and g_s (3rd column) from 2006-2012. The rows represent the *limited nitrogen* (row 1), *unlimited nitrogen* (row 2), and *no downregulation discrimination* (row 3) simulations. The black line in the 1st column is based on exponential fitted line from observed relationship at Niwot Ridge (Bowling et al. 2014). The horizontal lines represent $\delta^{13}C$ of 17 ‰ and are included for reference.